

UNCLASSIFIED



Australian Government
Department of Defence
Science and Technology

Computational model development for Additive Manufacturing (AM) based laser cladding structural repairs of high strength metallic aerospace components

Kevin Walker DST Group

Tim Cooper QinetiQ

Ondrej Muransky and Phil Bendeich ANSTO

ADF Aircraft Structural Integrity Symposium (AASIS) 18-20 March 2019



DST Science and Technology for Safeguarding Australia

Acknowledgements

Thanks to

- Dr Scott Walker and Mr Dan Galea from IR Signatures Group at DST
- Prof Milan Brandt and Dr Cameron Barr from RMIT Centre for Advanced Manufacturing
- Dr Qianchu Liu DST Group for support to Laser Cladding research and development

Presentation Outline

- Aim
- Why Laser Cladding (LC)?
- Previous work with AerMet[®]100 Steel
- Modelling residual stress – 4340 steel
- Accounting for phase change effects
- Comprehensive investigation into 316L and 300M steels
- Conclusion and ongoing/future work
- Questions

Aim: Develop certified, structurally significant repairs for high strength steel components such as landing gear



<https://www.nwfdailynews.com/news/20180822/nose-down-f-35-grounded-during-investigation-second-f-35-suffers-bird-strike>

Example case: F-35 NLG Piston, 300M Steel



Why Laser Cladding as a repair technology?

- Makes repair of expensive components possible
- Can repair components when lead-time may be excessive
- Can improve performance of the part



Liu, Q., Janardhana, M., Hinton, B., Brandt, M., and Sharp, P., *Laser cladding as a potential repair technology for damaged aircraft components*, in *International Journal of Structural Integrity*, 2011. 2(3): pp. 314-331.

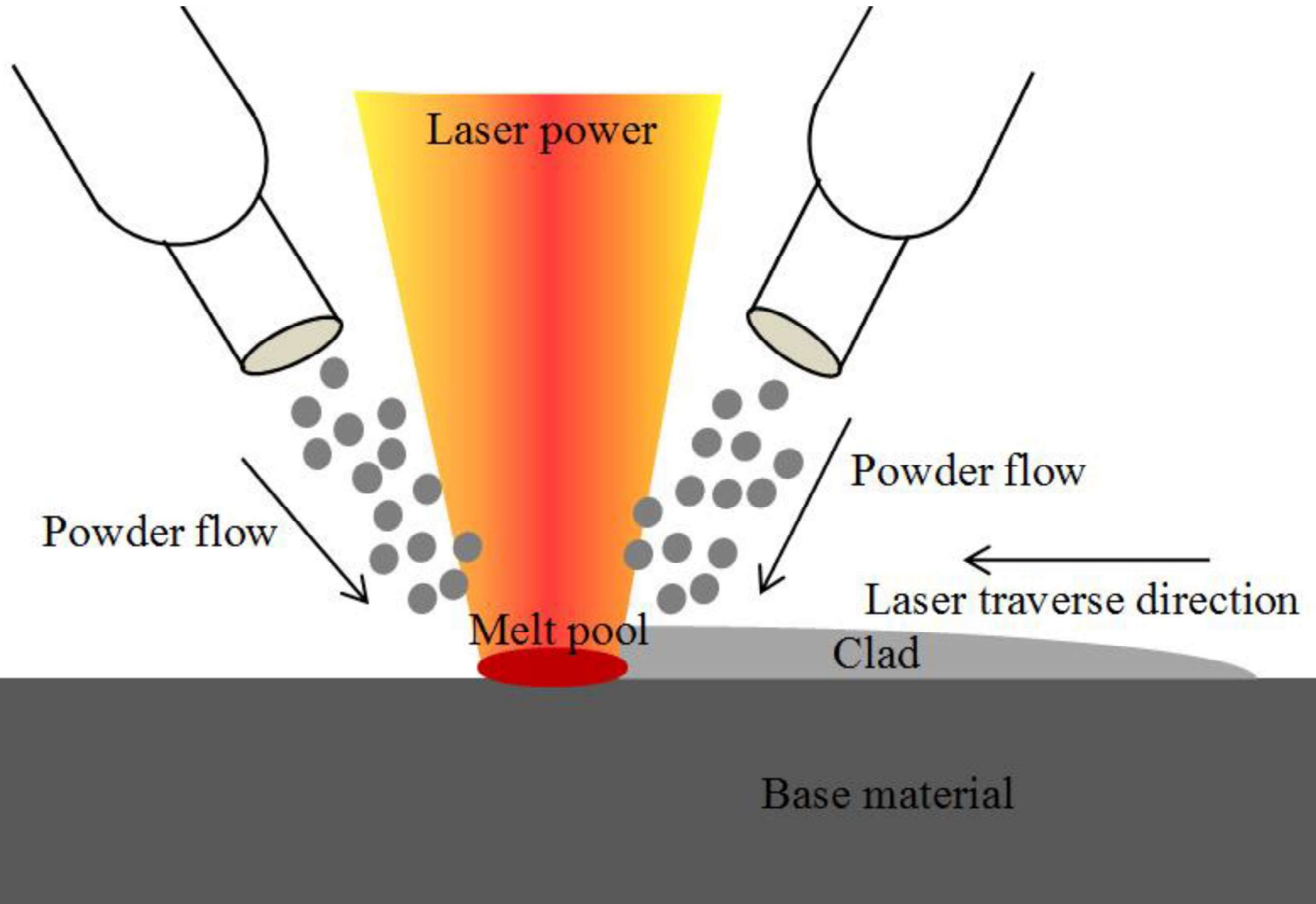
Liu, Q., Walker, K.F., Djugum, R., and Sharp, P.K., *Repair of Australian military aircraft components by additive manufacturing technology*, in *NATO Specialists Meeting on Additive manufacturing for Military Hardware*. 2016: Tallinn, Estonia.

Liu, Q., Djugum, R., Sun, S., Walker, K., Choi, J., and Brandt, M., *Repair and Manufacturing of Military Aircraft Components by Additive Manufacturing Technology*, in *17th Australian Aerospace Congress*, 2017: Melbourne, Australia.

Advantages of Laser Cladding

- Low dilution and heat input
- Low material distortion
- Low porosity, no micro-cracking, minimal heat affected zone, no or minimal damage to the substrate
- Good metallurgical bond
- Good mechanical properties
- Powder blend and process can be managed to achieve desired mechanical properties

Laser Cladding Process



Two categories of repair

Geometry restoration

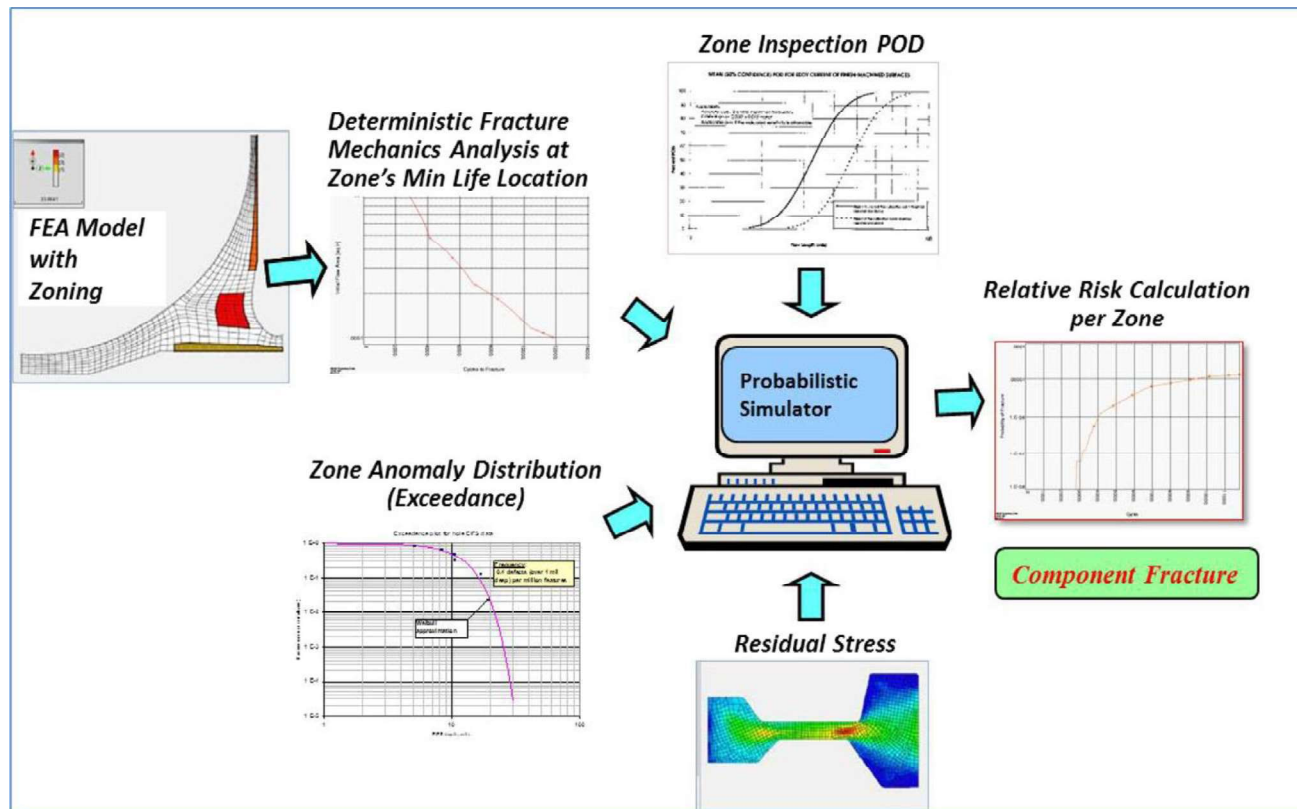
- Residual strength and fatigue life not compromised by the damage
- Repair needed to restore:
 - Form, fit and function
 - Corrosion protection
 - Surface finish

Structural

- Damage is such that static strength and/or fatigue life margins are compromised
- Need to demonstrate that the repair restores structural integrity, in addition to the geometry restoration requirements

Design, Substantiation and Certification - Structural Repairs

- High fidelity, accurate modelling essential
- Key aspects include:
 - Residual stress
 - Crack propagation

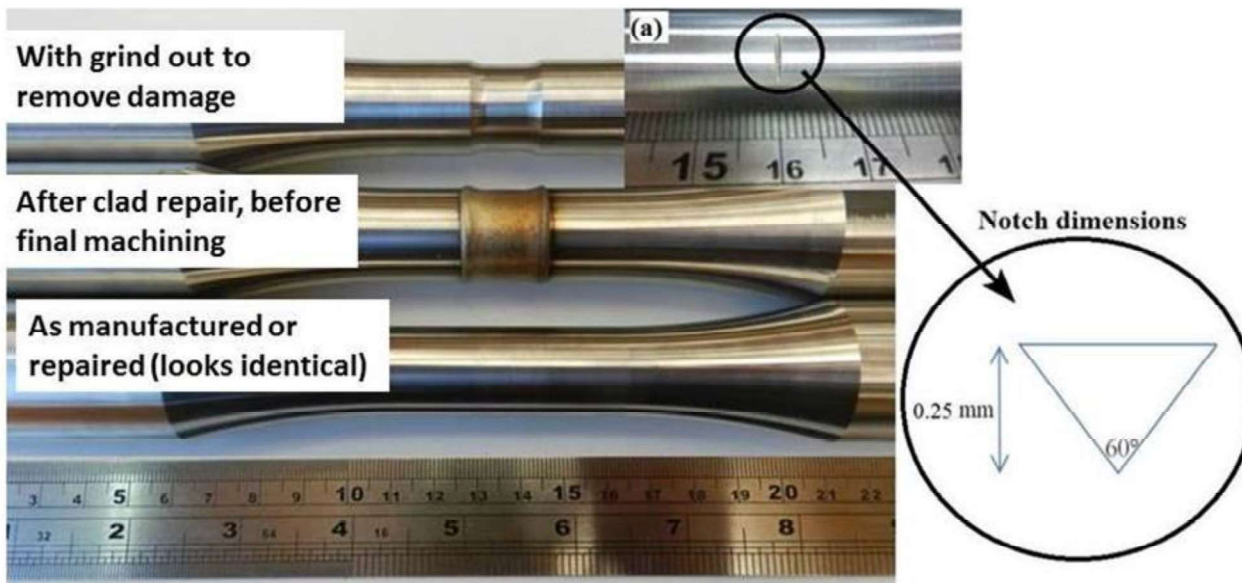


Source: Gorelik, M., International Journal of Fatigue 94 (2017) 168-177

Previous work with AerMET[®]100 Steel

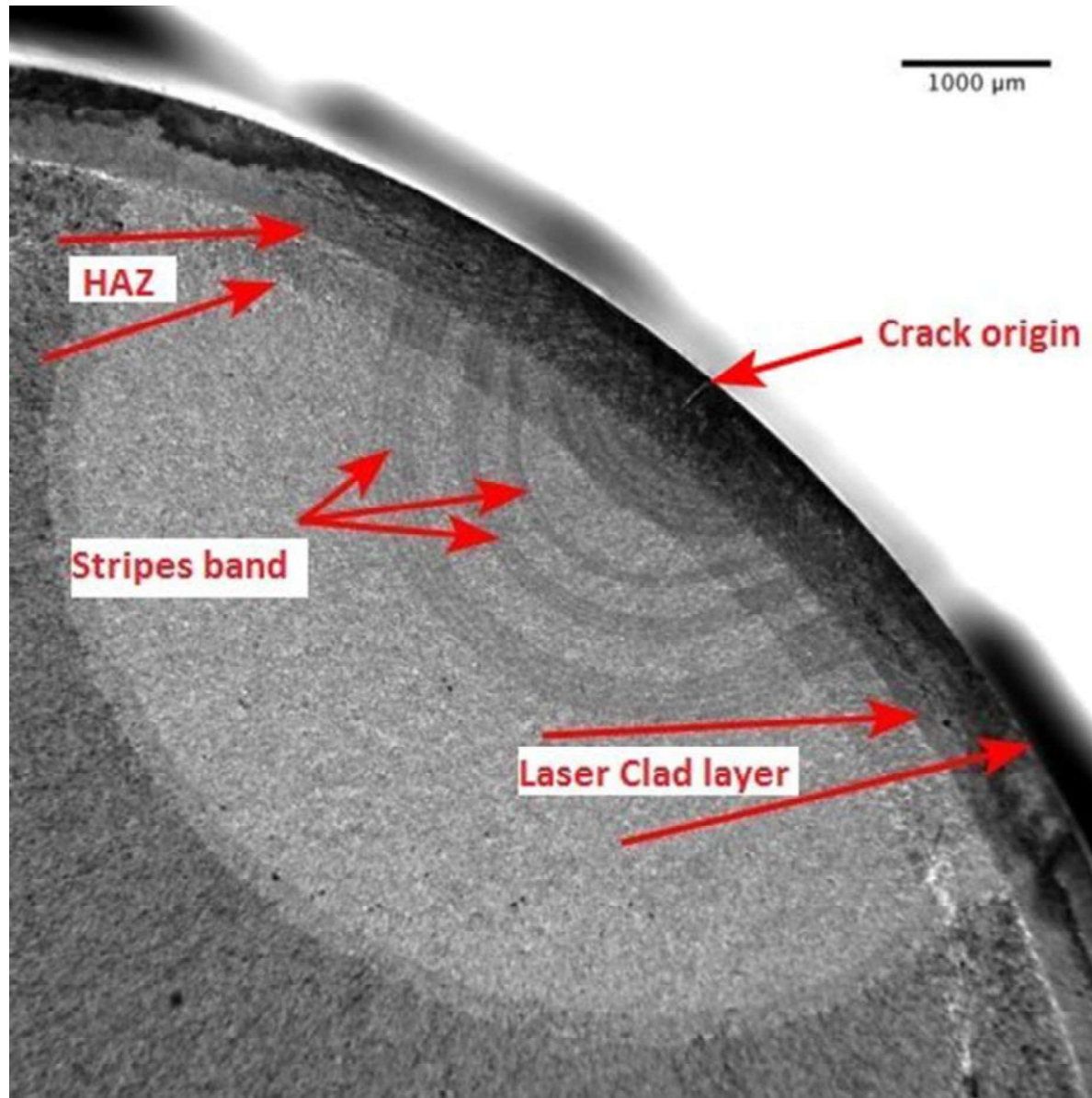
Structural Repair of AerMet[®]100 Steel

- AerMet[®]100 32/20 mm dia round bar samples
- Baseline: no repair, with 0.25 mm deep crack starter
- Repair: 0.5 mm deep, 10 mm long groove, repaired by cladding with TRUMPF TrueLaser Cell 7020 System, without crack starter

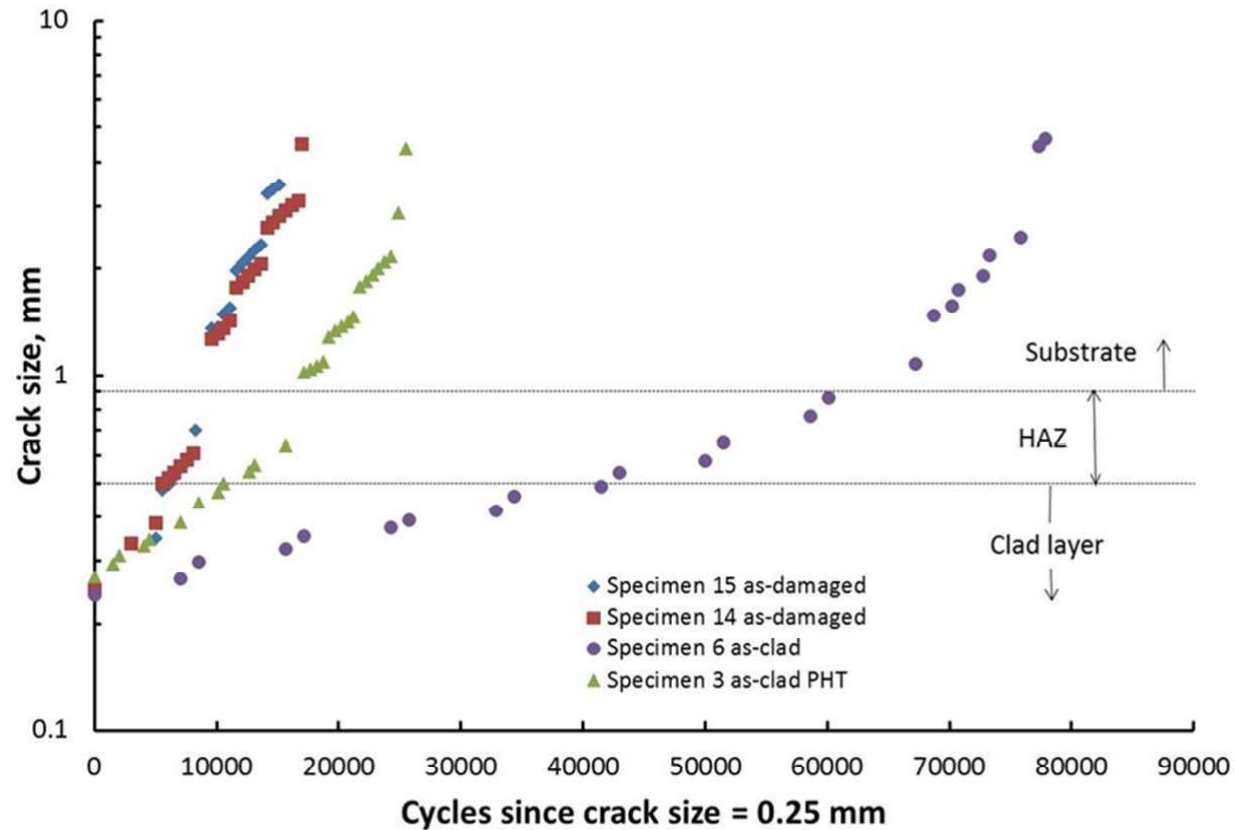


Walker, K.F., Lourenco, J.M., Sun, S., Brandt, M., and Wang, C.H., *Quantitative fractography and modelling of fatigue crack propagation in high strength AerMet100 steel repaired with a laser cladding process*. International Journal of Fatigue, 2017.

Test Results : As-clad



Test Results – Comparison of all three test cases

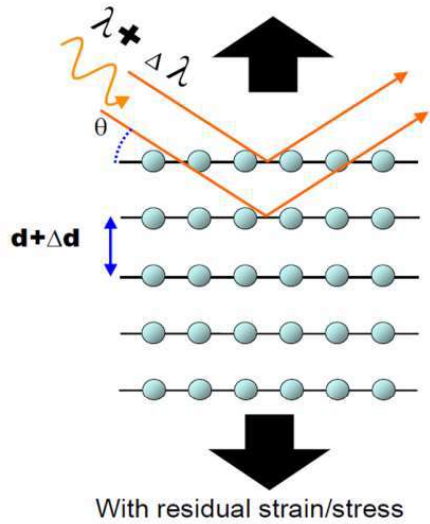


- Clad repair - fatigue crack growth life improvement by more than a factor of four
- Due to beneficial residual compressive stress
- Crucially important to understand and quantify those residual stresses in order to accurately model the process

Residual stresses measured by three methods

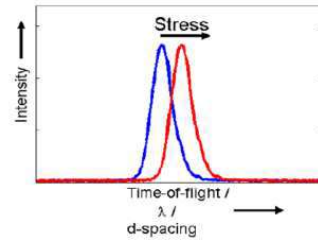
- Neutron diffraction

- X-ray diffraction

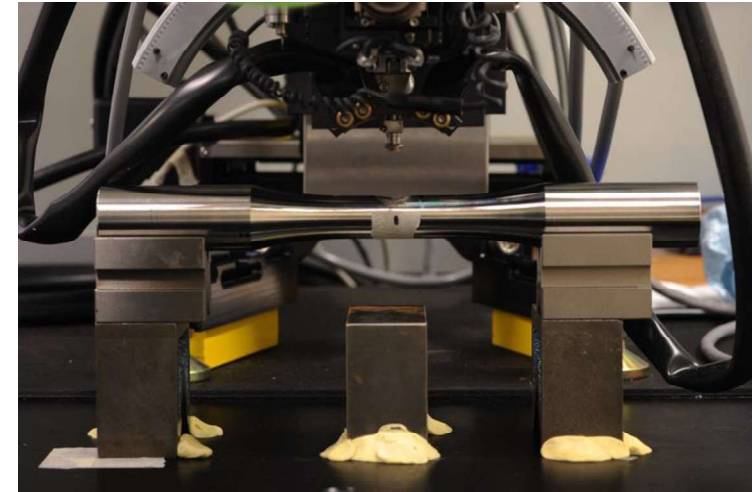


Bragg's Law:
 $d = \lambda / (2 \sin \theta)$

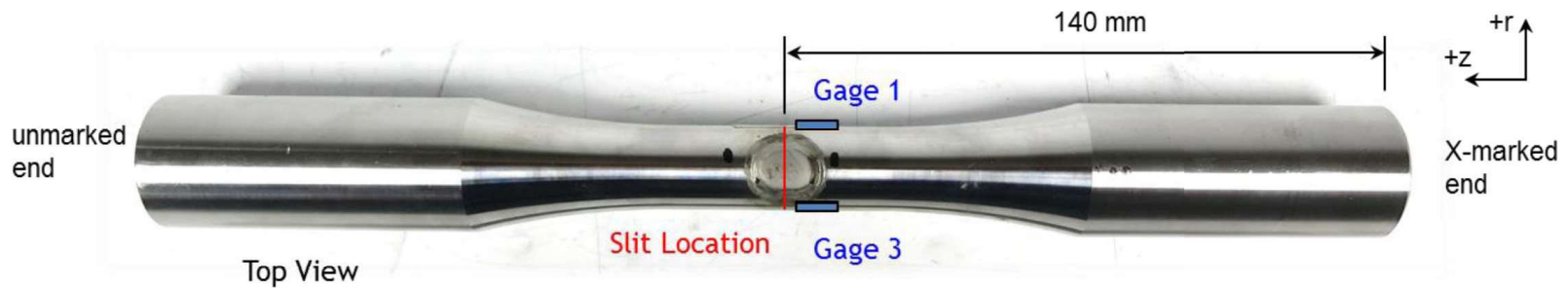
Fixed angle θ : $\epsilon = \frac{\Delta d}{d} = \frac{\Delta \lambda}{\lambda}$



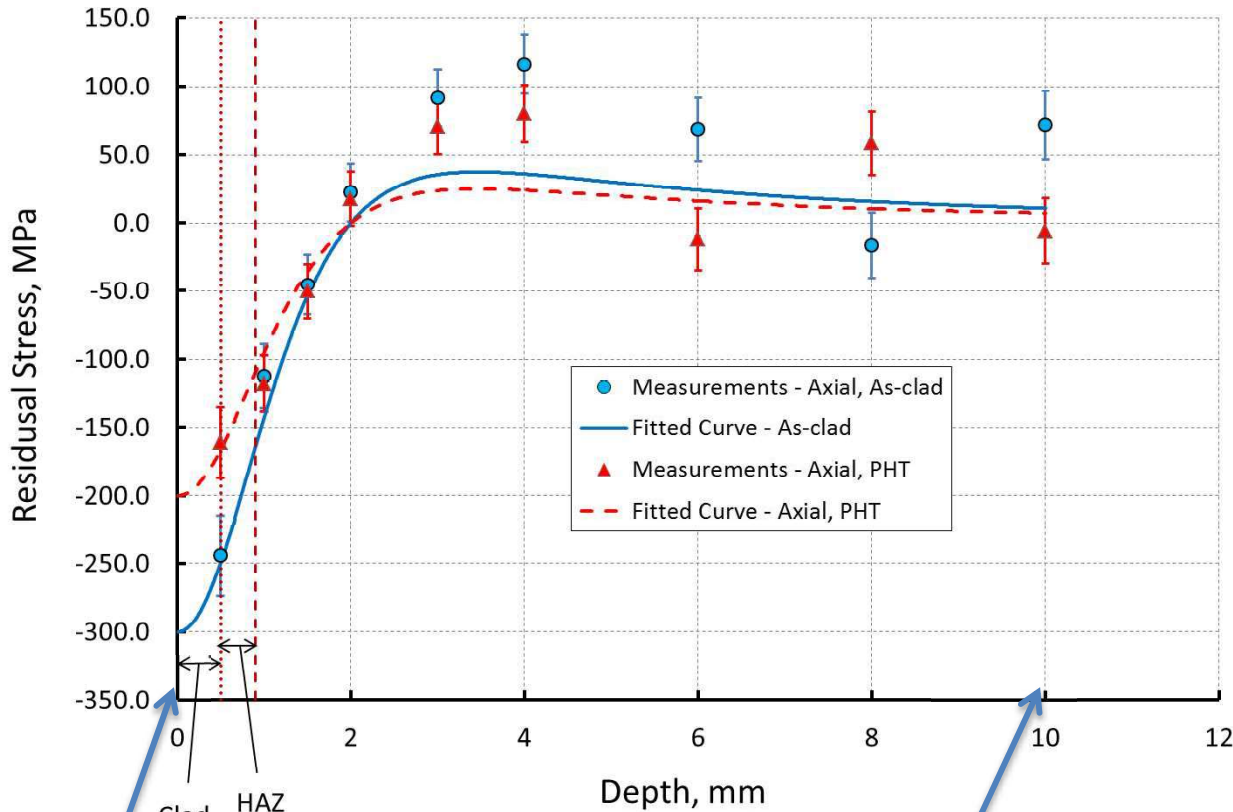
Diffraction peak shift is used to determine residual strain and stress



- Slitting

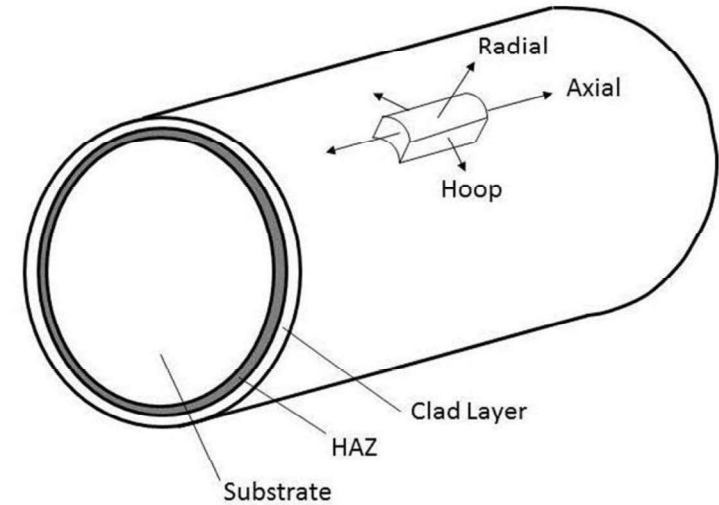


Residual Stress Measurement – Neutron Diffraction



Surface

Centre

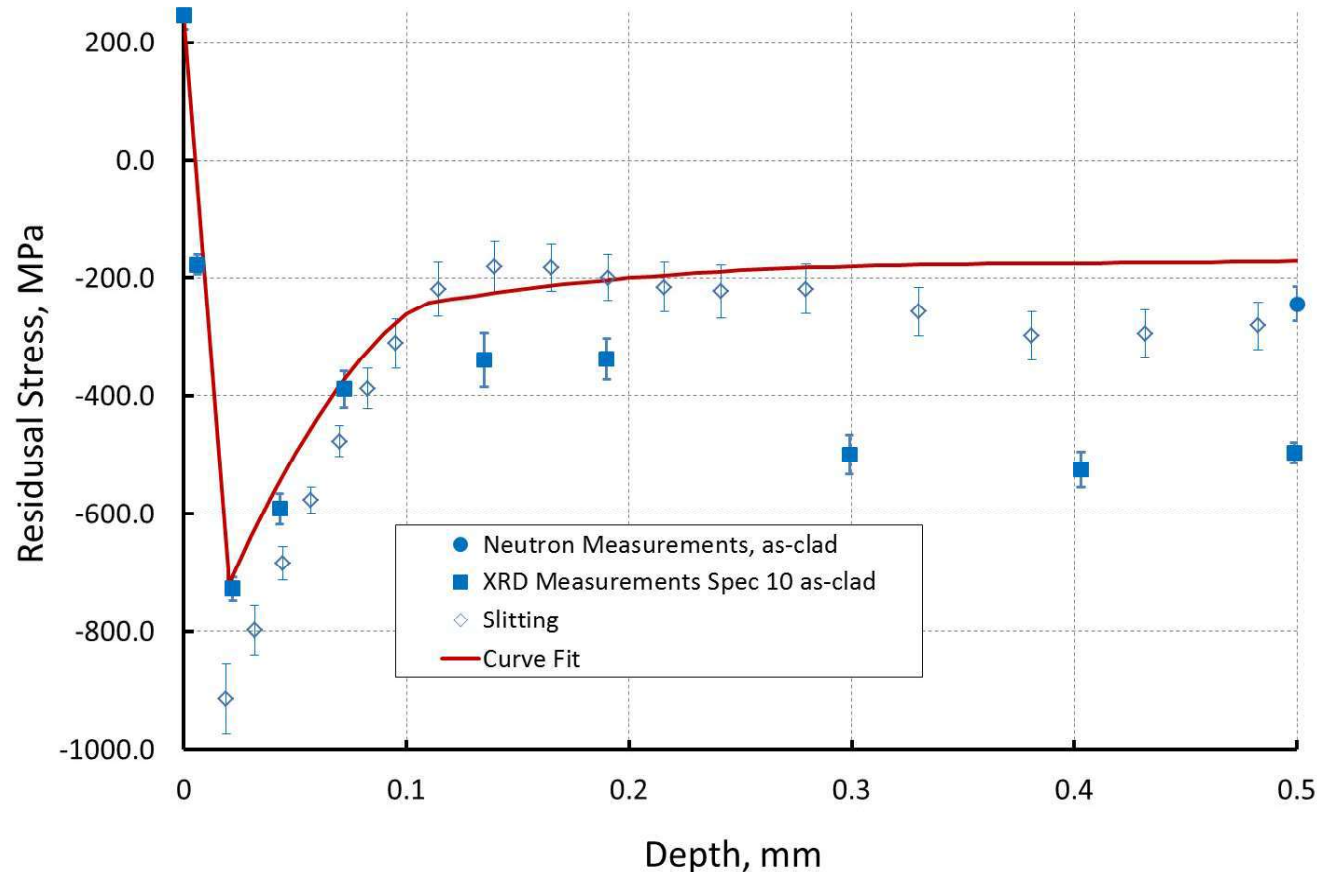


$$\sigma_R(z) = \sigma_{R,max} \frac{1 - (z/d)^2}{[1 + (z/d)^2]^2}$$

Satisfies the zero net force condition


$$\int_0^{\infty} \sigma_R(z) dz = 0$$

Neutron, X-Ray, Slitting Results – Clad Layer



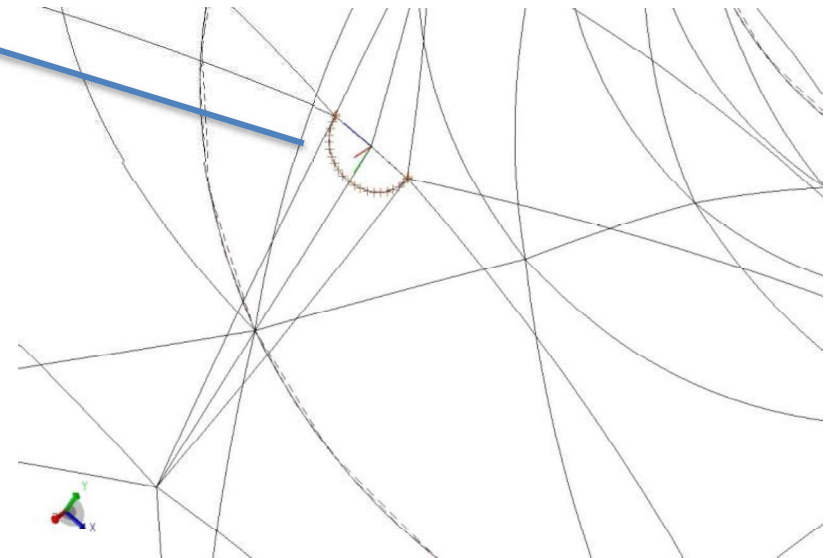
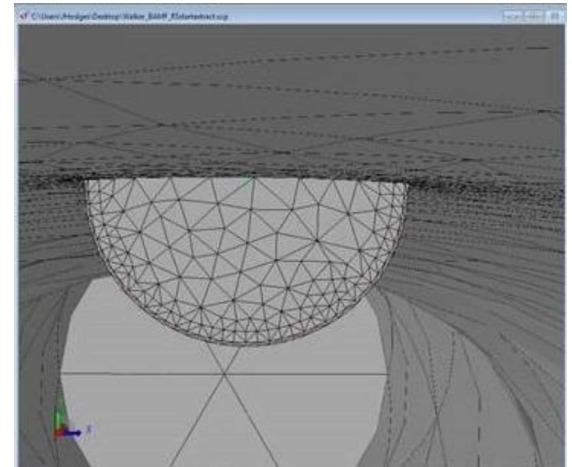
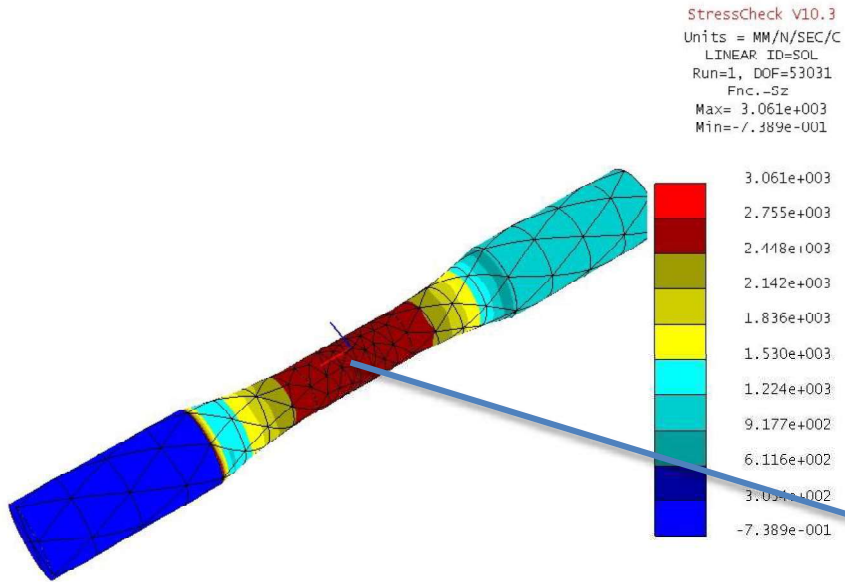
- Shown for the area of interest near surface, in the clad layer
- Some disagreement between X-Ray and slitting, but slitting agreed better with neutron result at 500 μm
- Slitting samples all around the circumference and gives an average result

BAMF/AFGROW/StressCheck Model

- BAMF – Broad Area for Modelling Failure
- USAF sponsored code, managed and being further developed/validated by Hill Engineering
- BAMF is a “plug-in” for the AFGROW fatigue crack growth analysis code
- StressCheck  p-element FE code used here for stress intensity factor (SIF) solution development
- StressCheck model runs to calculate SIF, this is fed to AFGROW for the crack growth (FASTRAN model in this case). Crack is grown by an incremental amount, and new shape returned to StressCheck to update SIF solution
- Iterative process continues to advance the crack through to final failure



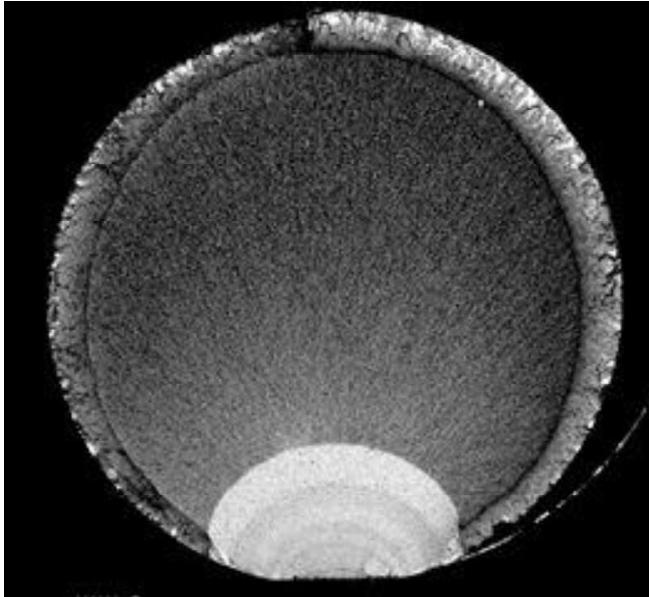
BAMF/AFGROW/StressCheck Model Overview 1



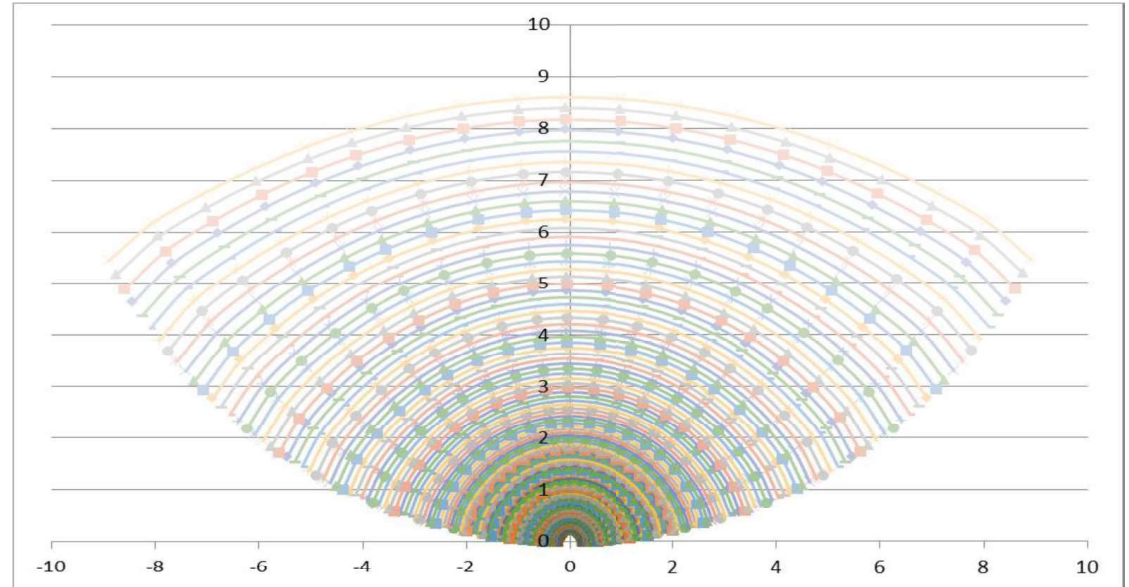
StressCheck FE Model

Crack Detail

BAMF/AFGROW/StressCheck Model Overview 2



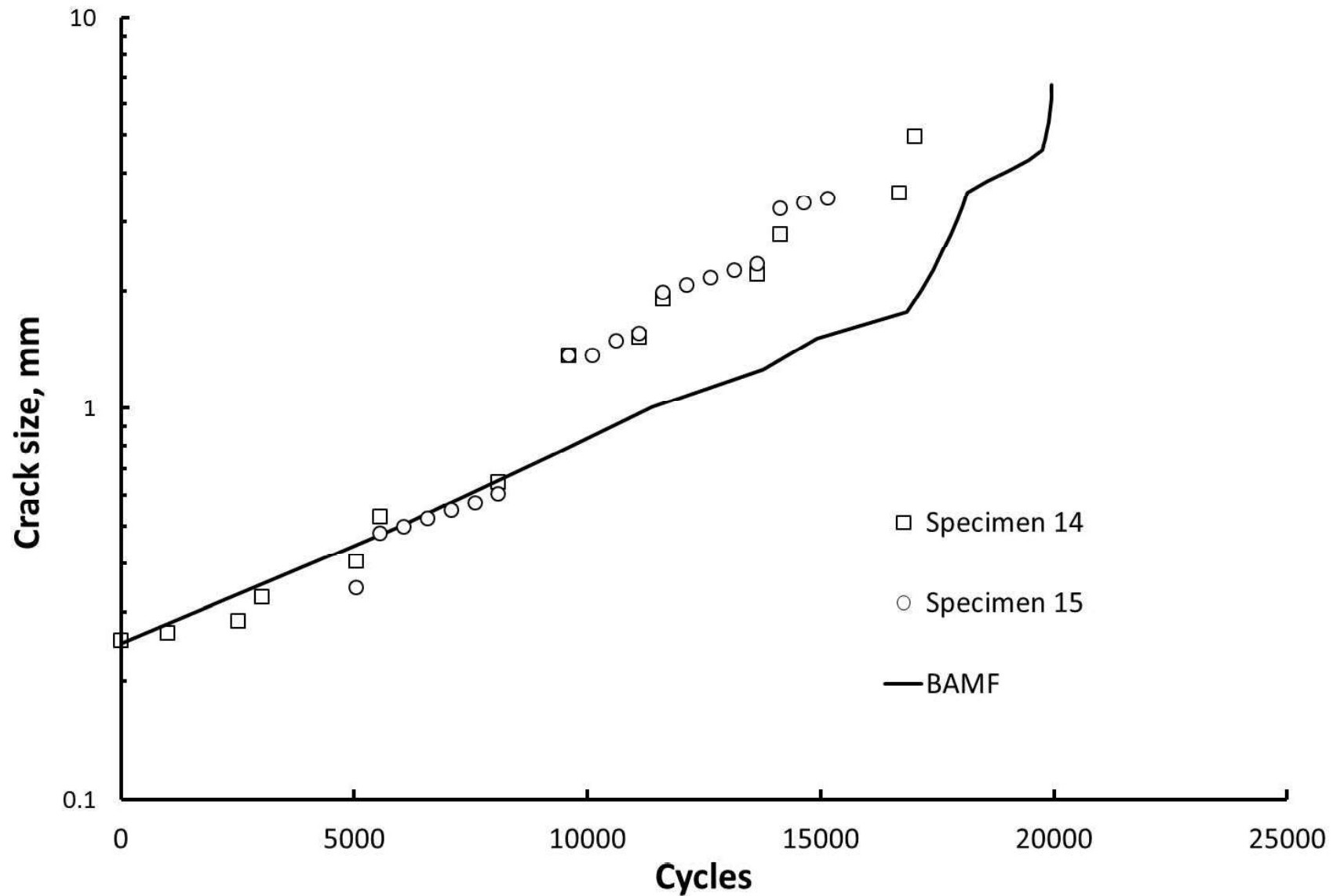
Crack Surface



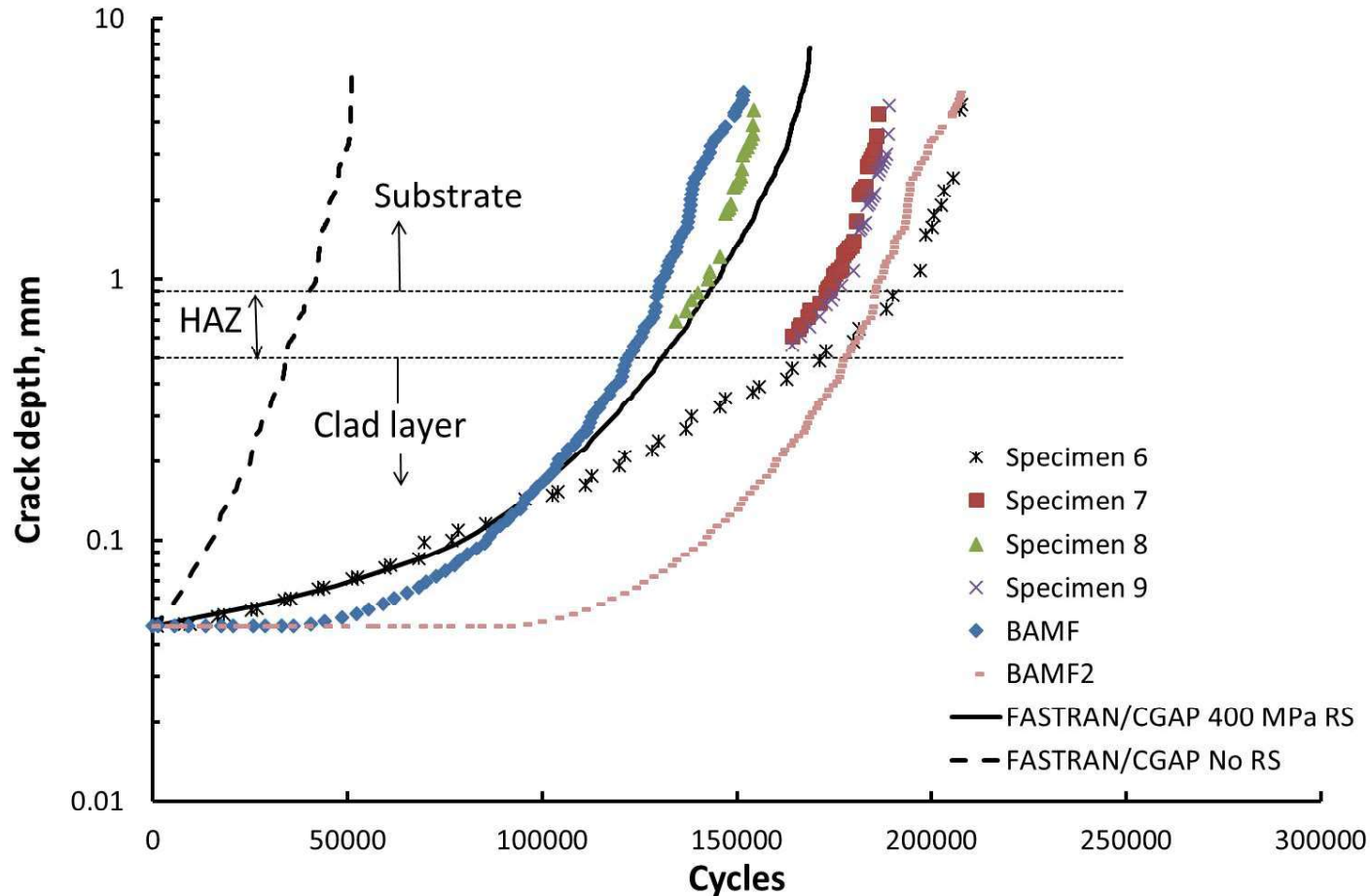
BAMF Crack Model

- SIF Calculated at 20 points around crack front
- Crack size incremented by 3% per step

Full BAMF Model Results : Baseline

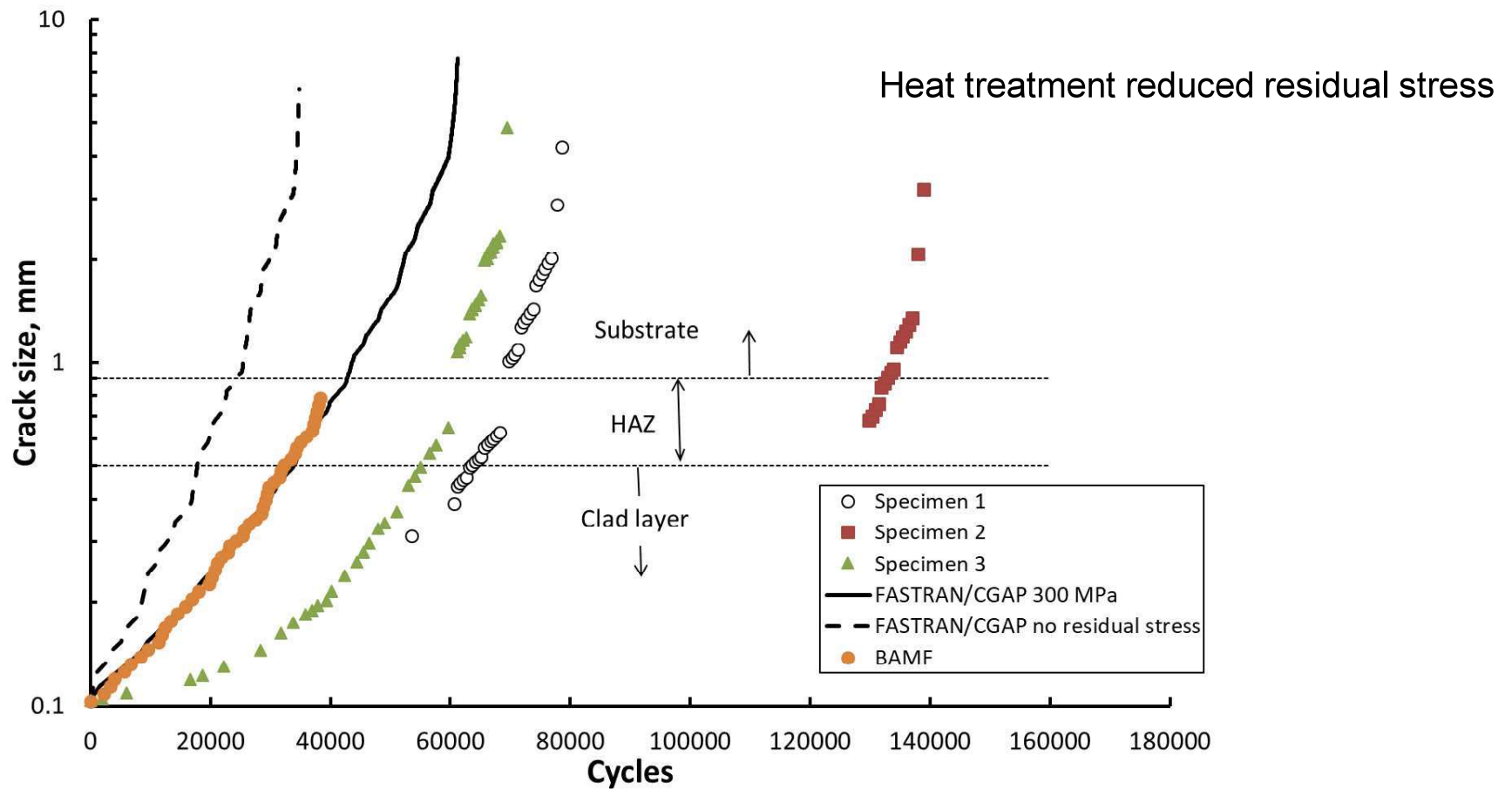


FASTRAN/CGAP/BAMF Modelling Results: As-clad



- Both BAMF and CGAP/FASTRAN modelling correlated well
- BAMF modelling still being reviewed, particularly in the early stage of growth

FASTRAN/CGAP Modelling Results: PHT



- Full BAMF modelling still in development/review
- BAMF results appear consistent with simplified FASTRAN/CGAP approach at this stage

Summary thus far with AerMet[®]100

- Can measure residual stress and crack growth
- Can model the crack growth, including through the residual stress field
- For a complete modelling capability, also need to model the residual stress field.

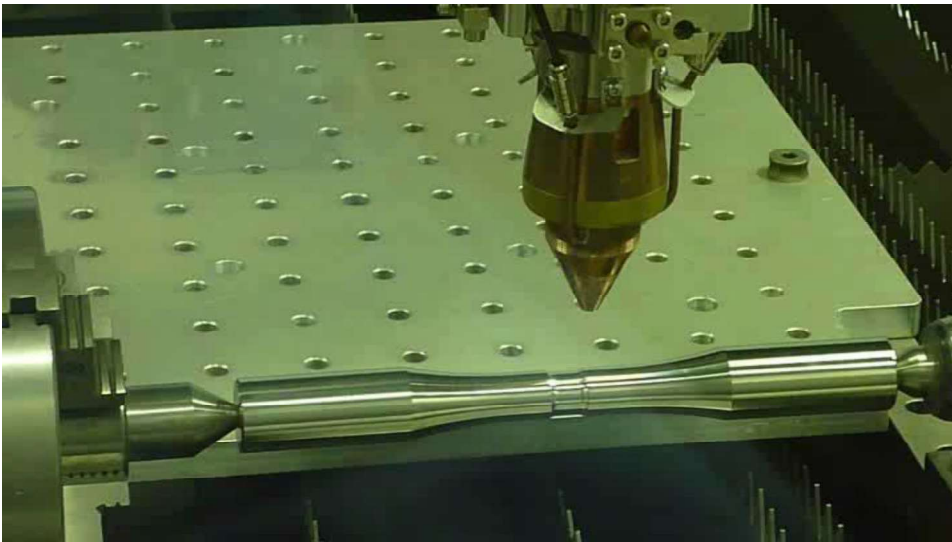


Aim – Modelling of the Residual Stress

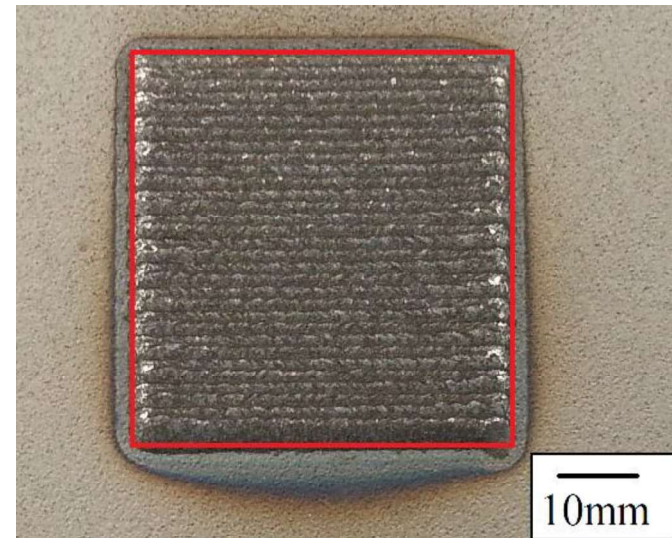
Develop a thermomechanical model of the laser cladding process

- For AerMet[®]100 Cylindrical Bar Test Specimens
- Start with AISI 4340 Steel Rectangular Plate Samples where test data (thermal profiles and measured residual stresses) available

AerMET[®]100

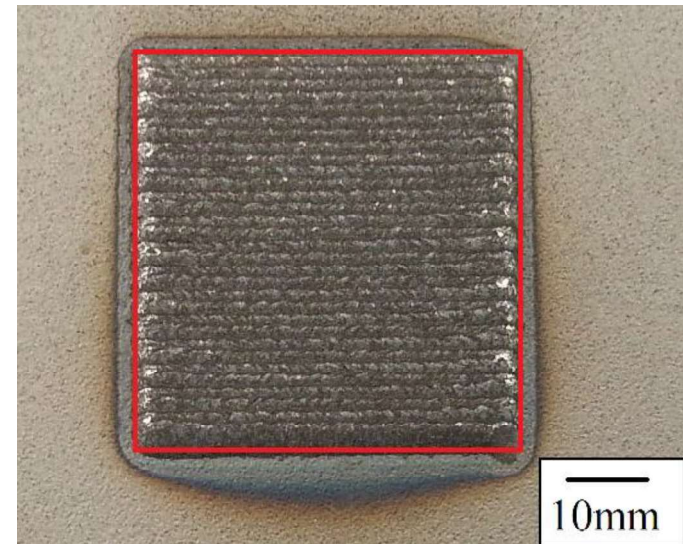
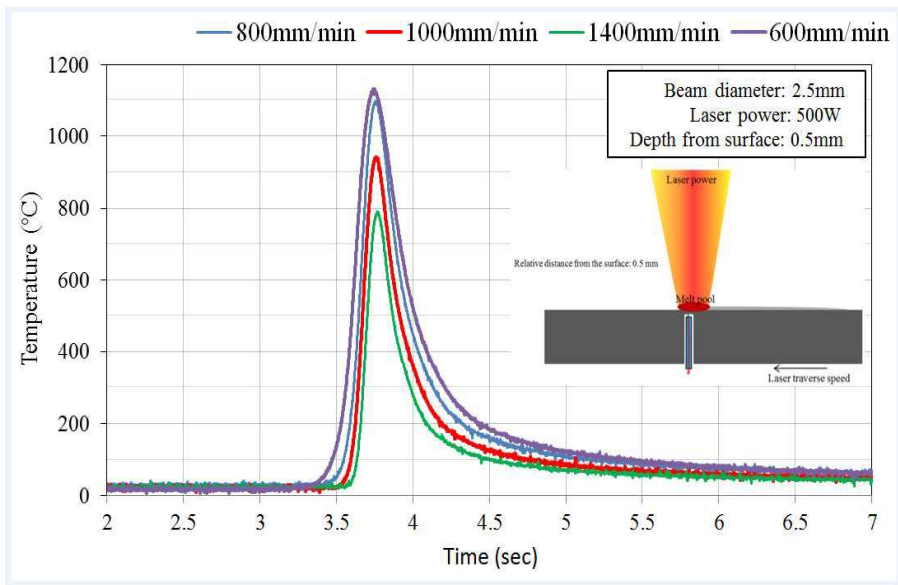


AISI 4340 STEEL



Experimental data available for 4340

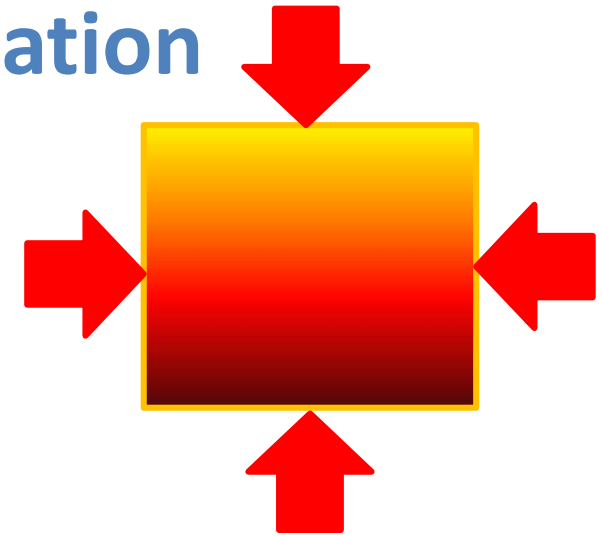
- Deposition experiments performed by S. Sun (RMIT) in collaboration with DST Group
- AISI 4340 steel plates (200 x 100 x 10)
 - Thermocouple experiments
 - No deposition
 - Temperature history at 0.5 mm depth
 - Residual stress experiments
 - AISI 4340 material deposited
 - Residual stress evaluation using Neutron Diffraction



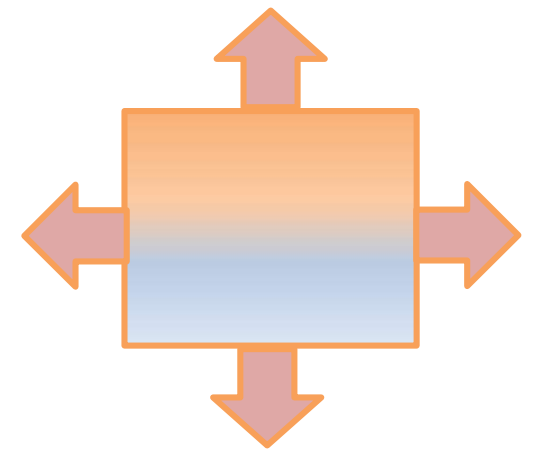
Mechanism of Residual Stress Formation

Residual stress state is primarily governed by plastic yielding under constrained transient thermal expansion and contraction.

It is anticipated that the highly local (to the laser heated melt-pool) effects of liquid metal flow need not be modelled discretely to capture the final residual stress state.



Constrained Expansion
under Heating

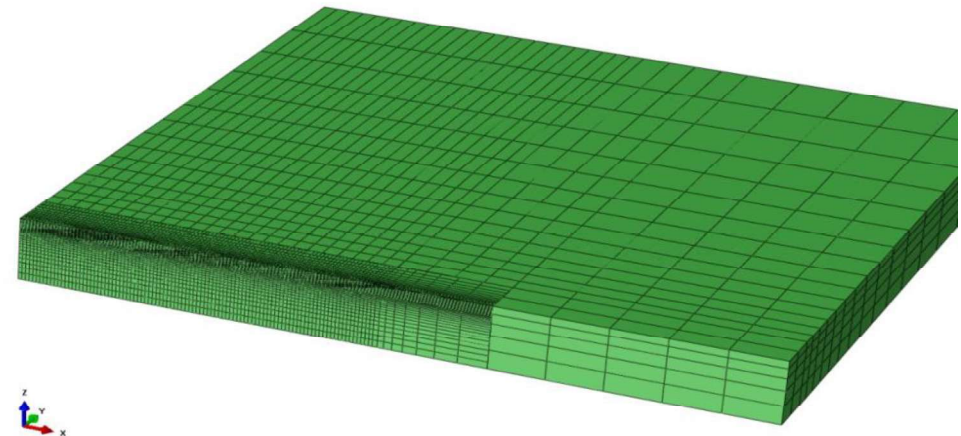
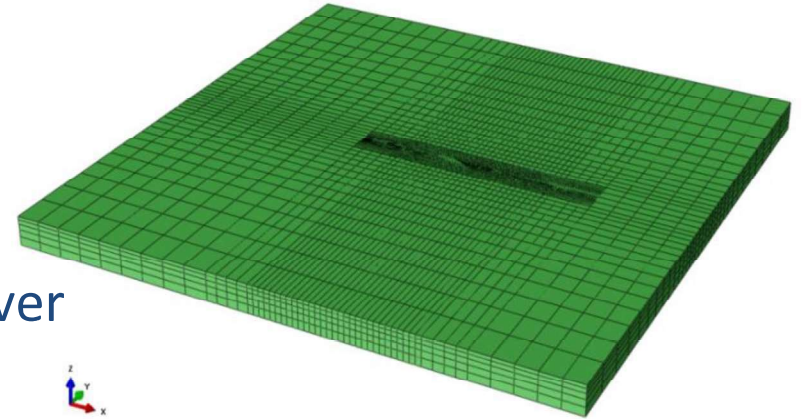


Constrained Contraction
under Cooling

Thermal Model

Transient Thermal Finite Element Analysis

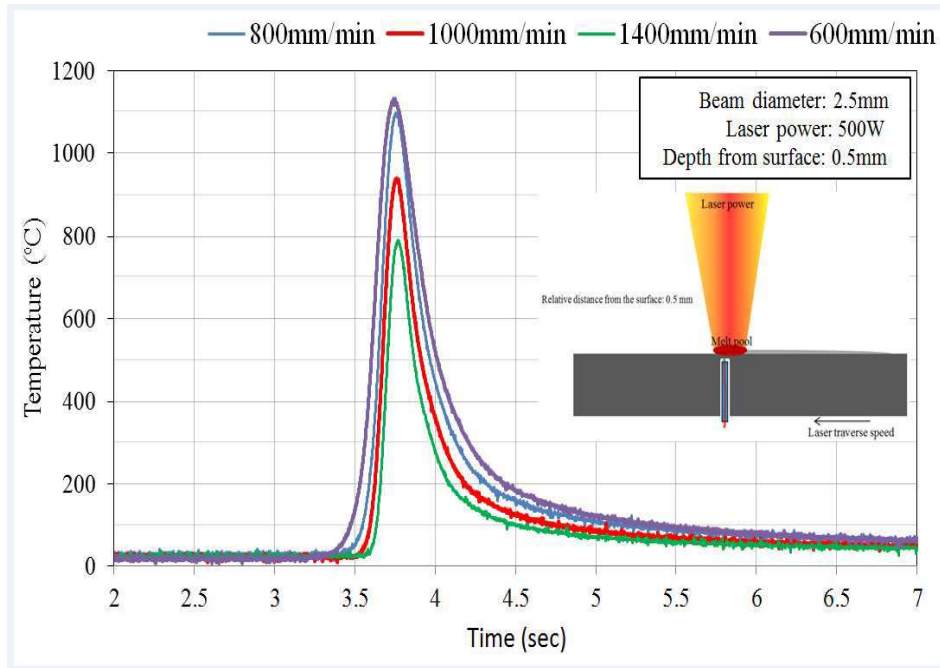
- ABAQUS 2016 Software
- Temperature field modelled using explicit solver
 - Decoupled from displacement field
- Thermal load scaled from laser beam profile interpolation
- Conduction out through Plate Supports shown to have negligible effects in the time-frame considered
- Convection & radiation heat transfer to ambient conditions ignored
- Total 7.5 second simulation
 - 2.5 second laser scan
 - 1400, 1000, 800, 600 mm/min
 - 5.0 second cool down



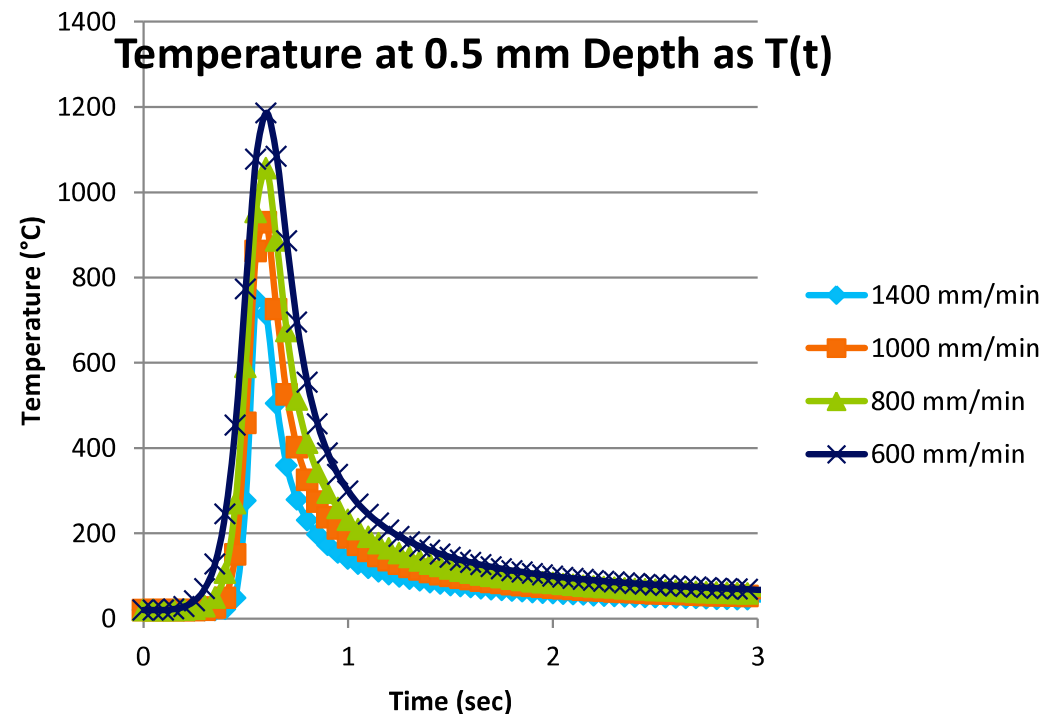
Thermal Model Correlation

- Single pass, no material deposition
- Strong agreement of temperature transients (rise/decay profiles and rates)
- Quantitative agreement to within 7 % against peak temperature
 - Achieved using heat source amplitude scaling
 - Equivalent to setting an effective absorptivity

EXPERIMENT

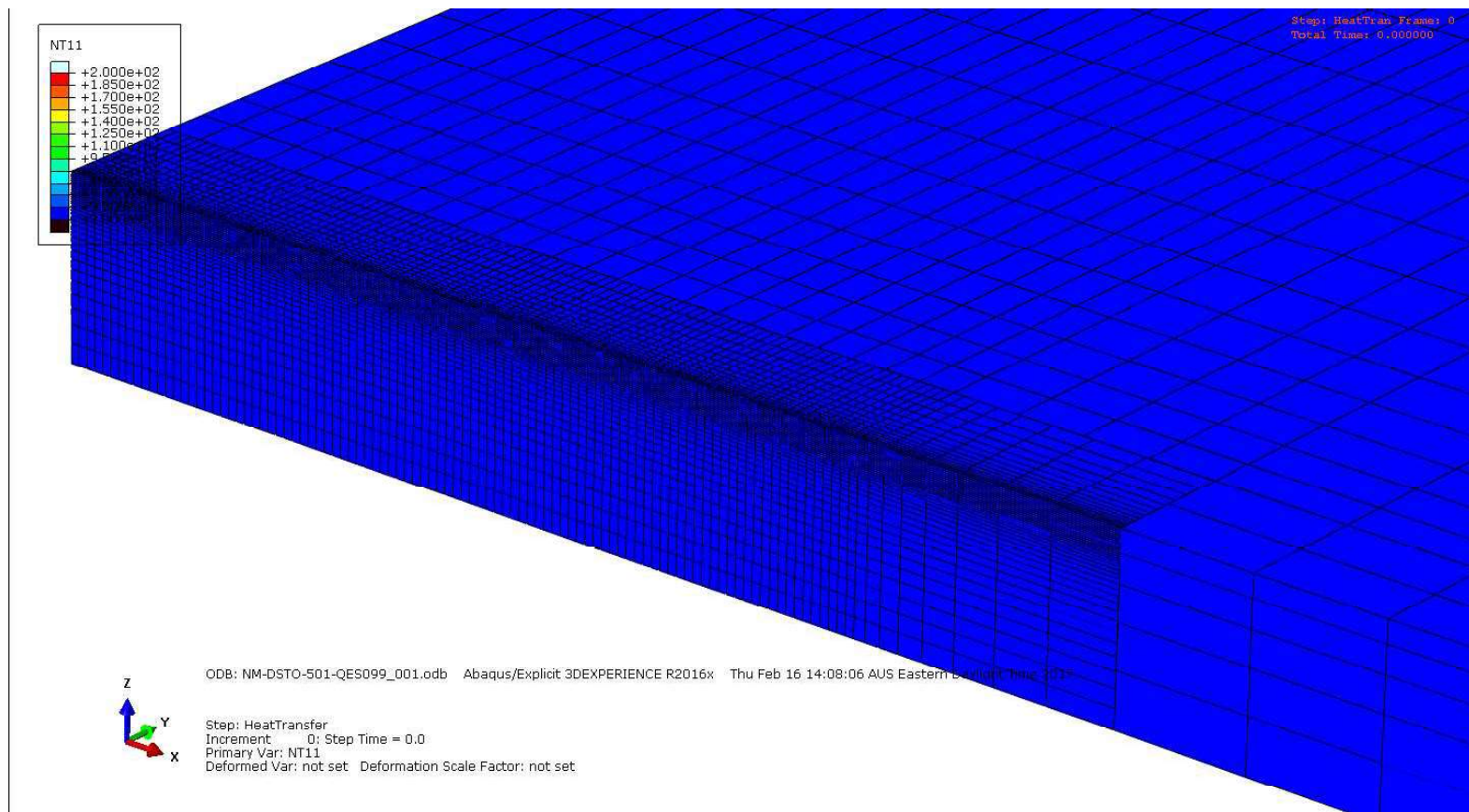


SIMULATION



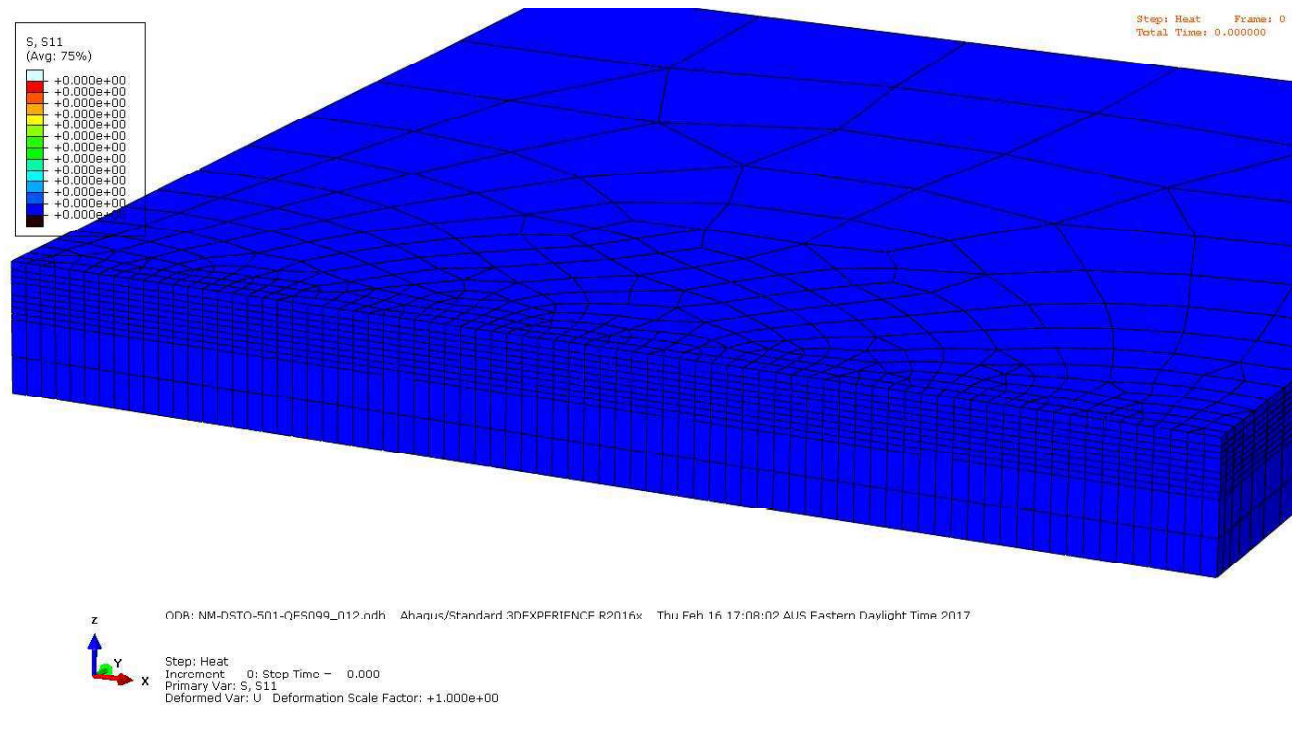
Thermal Analysis – Results

AISI 4340 Plate Quarter Model – 0 to 200°C
Temperature Range



Residual Stress Analysis - Results

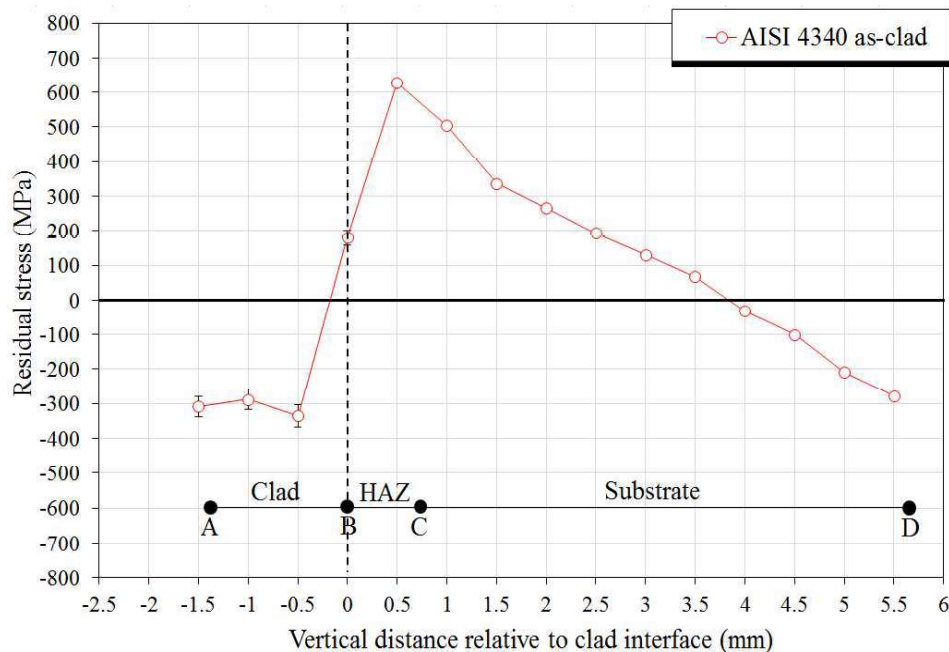
- Displacement (strain) field modelled using ABAQUS 2016 implicit solver
- Sequentially coupled to temperature field
- Distributed time-point body temperature from transient thermal analysis
- Stress development from constrained thermal expansion/contraction
- Total 7.5 seconds of simulation



Residual Stress Model Correlation

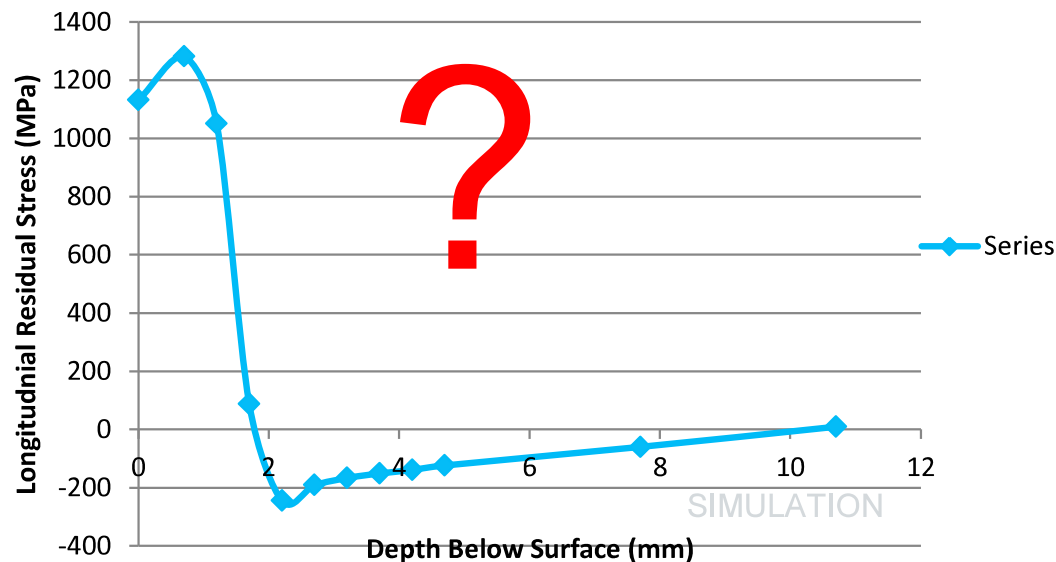
- Measured and modelled residual stress profiles are different. Why? Where did we go wrong?
- We did not model addition of material, or multiple passes. However, we believe there is something else even more important which we haven't accounted for.

EXPERIMENT



SIMULATION

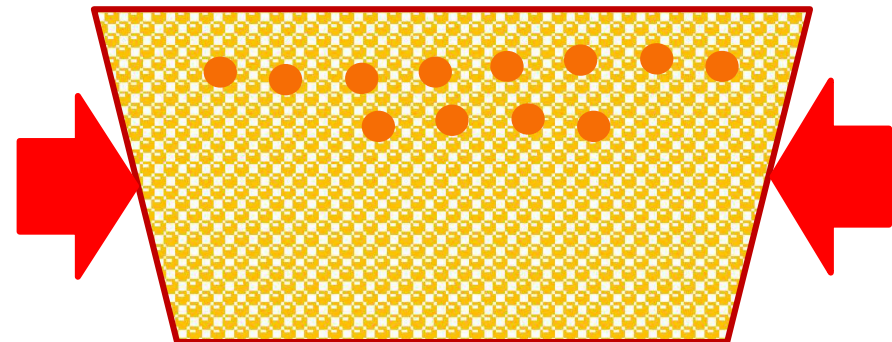
Longitudinal Residual Stress Variation with Depth



Evaluation- What's Happening?

- Residual stress can be driven by two mechanisms
 - Constrained thermal expansion and contraction, plus local material yielding
 - Phase transformation, with associated step volume changes
- For cases dominated by thermal expansion – results in primarily tensile residual stresses at the surface
- For cases dominated by material phase change – results in primarily compressive residual stresses at the surface (when phase change on cooling results in volume increase)
- A given material may be subject to both effects, given the right temperature and transient temperature conditions
 - This varies from point to point in test article
 - Being a function of local temperature, local temperature transients and bulk material constraint
 - Also a function of material composition, heat treatment history

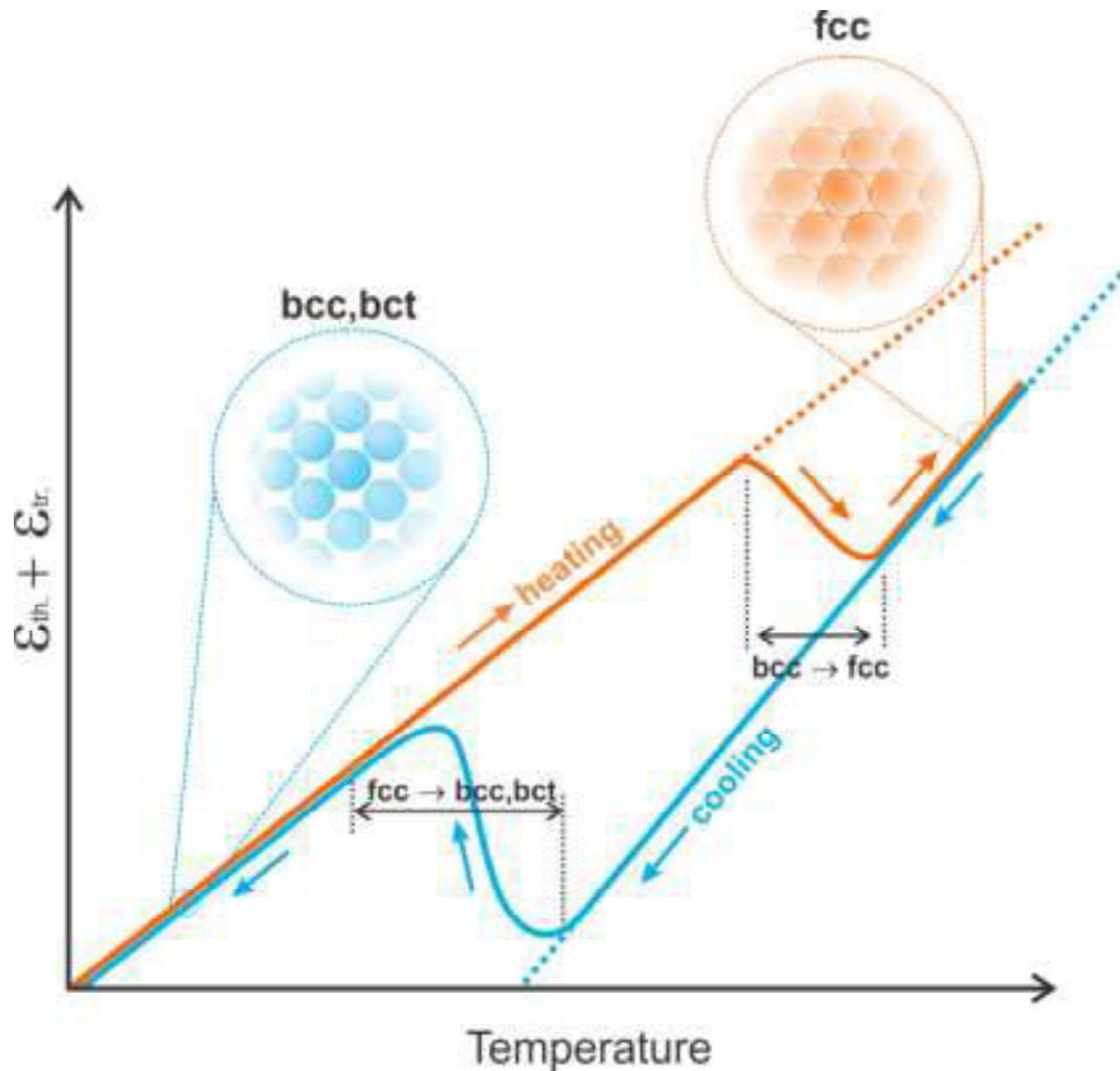
However, current model does not include the added material



Development of Model Accounting for Phase Change Effects

- Entered collaboration with ANSTO (Dr Ondrej Muransky and Dr Phil Bendeich)
- Devised heavily instrumented baseline experimental program on two steels:
 - 316L Austenitic Stainless Steel (no phase change)
 - 300M Ultra-high strength steel (undergoes Phase change to Martensite)
- Addition of ANSTO phase change model to existing QinetiQ/DST model. Initially for 4340 case, then to be extended to 300M

Accounting for Solid State Phase Transformation (SSPT)



ANSTO SSPT Model

SimCCT - Solid State Phase Transformation (SSPT) tool, v1.24 beta (13th Feb 2019)

File Edit Tools Help

Mode Alloy Analysis Ae3 Equil. Dilatometer

Setup

Composition (Steel), wt. %
 AISI 4340 Database diagram 5028

Select alloy
 Alloy-1 Alloy-2
 Diluted mix

Alloy-1 Alloy-2 mix composition

| | | | |
|---------|----------------|------|-------|
| 0.4 | Carbon, C | 0 | 0.044 |
| 0.035 | Phosphorus, P | 0 | 0.0 |
| 0.7 | Manganese, Mn | 0 | 1.730 |
| 0.23 | Silicon, Si | 0 | 0.220 |
| 1.83 | Nickel, Ni | 0 | 0.000 |
| 0.8 | Chromium, Cr | 0 | 0.000 |
| 0.25 | Molybdenum, Mo | 0 | 0.260 |
| 0 | Aluminium, Al | 0 | 0.0 |
| 0 | Copper, Cu | 0 | 0.0 |
| 0 | Arsenic, As | 0 | 0.0 |
| 0 | Titanium, Ti | 0 | 0.0 |
| 0 | Cobalt, Co | 0 | 0.000 |
| 0 | Vanadium, V | 0 | 0.0 |
| 0 | Tungsten, W | 0 | 0.0 |
| 0.04 | Sulphur, S | 0 | 0.0 |
| 0 | Nitrogen, N | 0 | 0.0 |
| 0 | Niobium, Nb | 0 | 0.0 |
| 0 | Boron, B | 0 | 0.0 |
| TOTAL % | | | |
| 2.25 | | 2.25 | 2.25 |
| 0.0 | Iron, Fe | 0.0 | 0.0 |

Method
 Kirkaldy (83)
 Li (98)

Grain Size, G
 0.02201 Dia. (mm)
 8 ASTM

Transformation % definitions
 0.1 % nucleation start
 0.99 % nucleation finish

Equilibrium Phase Fractions
 Auto calculate
 0.4722 **X_{Fe}**
 0.012 **CF (wt%)**
 0.77 **Co_{eff} (wt%)**

Transformation temperature limits
 Bainite / Martensite start and stop
 Auto calculate method
 303 MS temp Kirkaldy
 524 BS temp Li 98
 Austenite start and stop temperatures
 Auto calculate
 699 Ae1, Austenite->Pearlite limit, (C)
 746.8 Ae3, Austenite->Fertite limit, (C)

Define cooling profile
 850 Start Temperature, C
 cooling rate -CCT user defined
 10 C/sec

CCT Phase fractions -USER

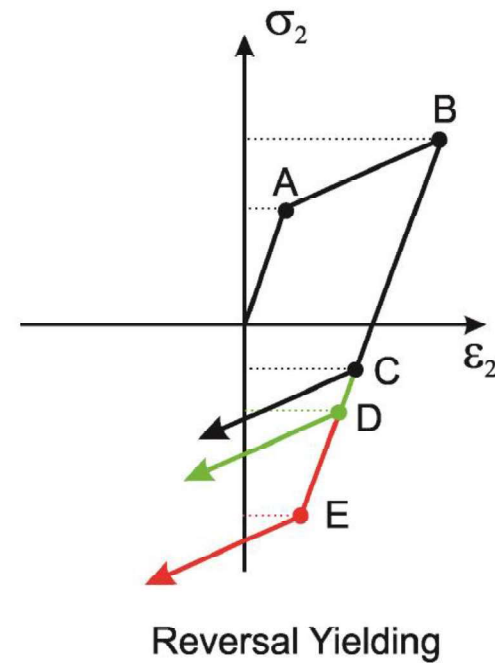
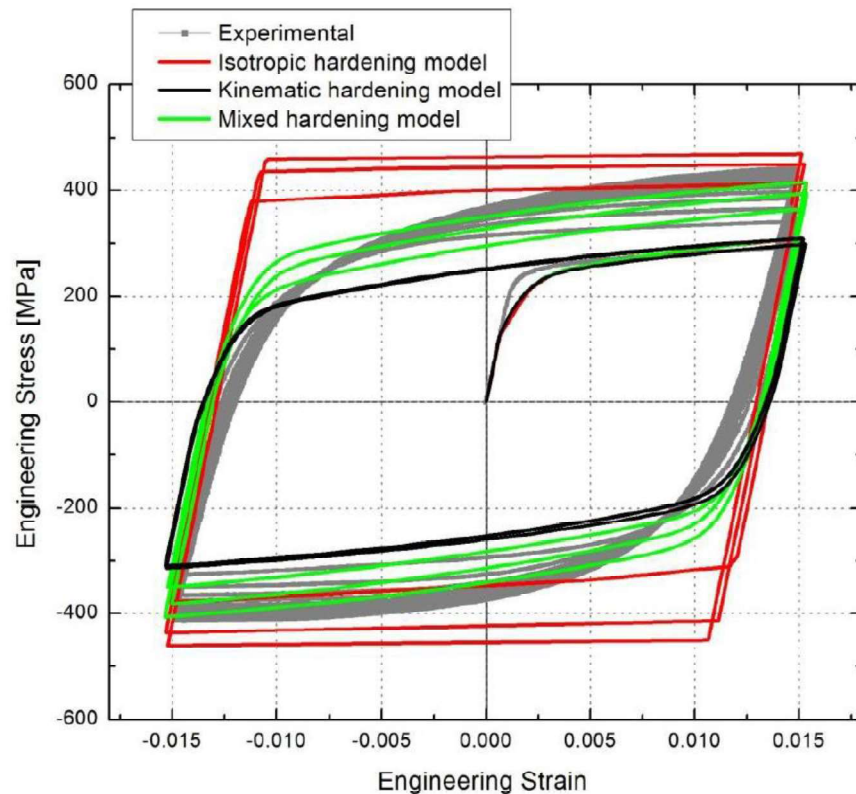
| | | |
|-------|------------|------------|
| 0.00 | Fertite | time (sec) |
| 0.00 | Pearlite | 74.6 |
| 48.42 | Bainite | C |
| 51.58 | Martensite | 104 |
| 0.00 | Austenite | |

TTT

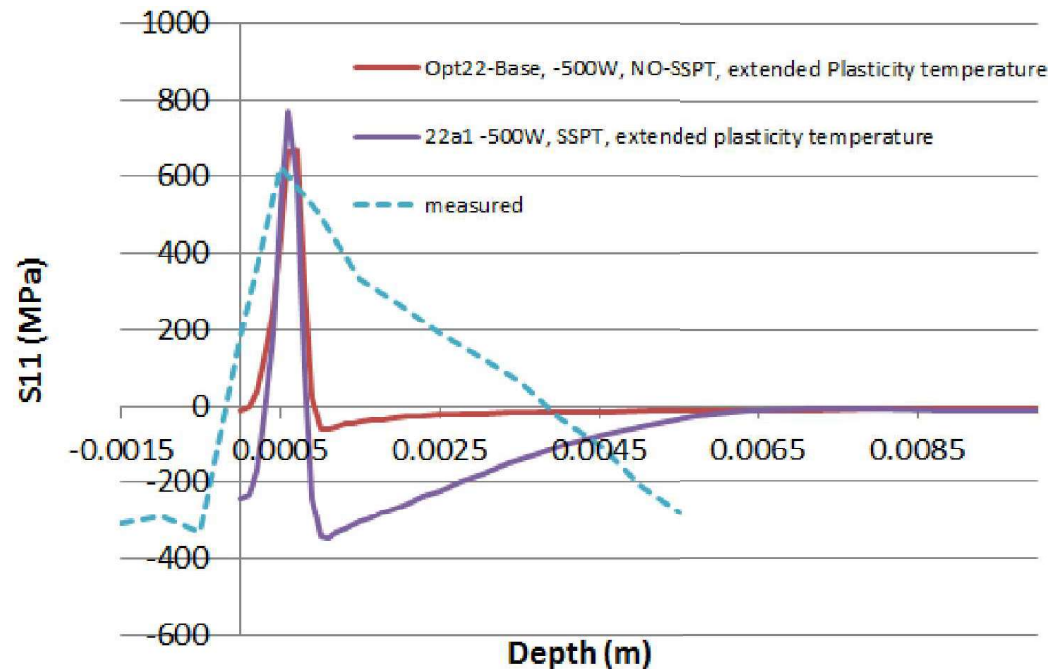
CCT

Hardening Model

- Material Model:**
- 1) Isotropic Hardening
 - 2) Kinematic Hardening
 - 3) Mixed (Isotropic-Kinematic) Hardening



Preliminary Results for 4340 Model with ANSTO SSPT Routine



- Do see compression when SSPT is included
- Several aspects not yet modelled, i.e.:
 - Deposition of material
 - Multiple overlapping passes

Comprehensive investigation into 316L and 300M Steels

- Experimental program
- Thermocouple measurements
- Infrared Camera Measurements
- Residual stress measurements including:
 - Contour
 - Neutron diffraction
- Metallography including:
 - Hardness maps
 - Microstructure and fusion zone assessment

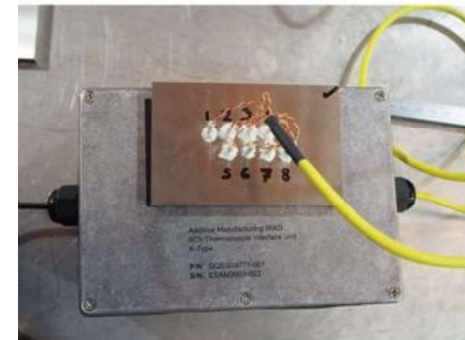
Experimental Program with 316L and 300M Steel

- 8 material samples for testing (4 x 300M, 4 x 316L)
- Mounting/retaining system to securely hold instrumented samples during the LD process
- Bespoke Data Acquisition Systems, each capable of logging 8 thermocouples at 100Hz for a five minute test period, one system per instrumented sample
- Tests of 8 material samples (4 x 300M, 4 x 316 S/S) undergoing LD in the Trumpf Laser at RMIT, Melbourne. Two of each material type were thermocouple instrumented, two were “dumb” samples subject to the same LD process. All samples were subjected to thermal imaging during the LD process
- Measurement of LD induced residual stresses in the “dumb” 300M and 316 Test Samples after LD, using 2 methods
 - The Contour (sectioning) method, and
 - The Neutron Diffraction method

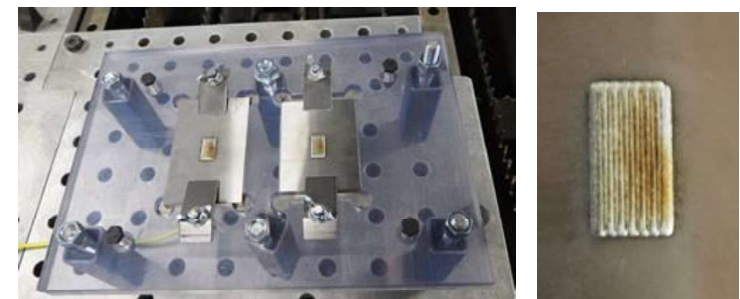
Mount System



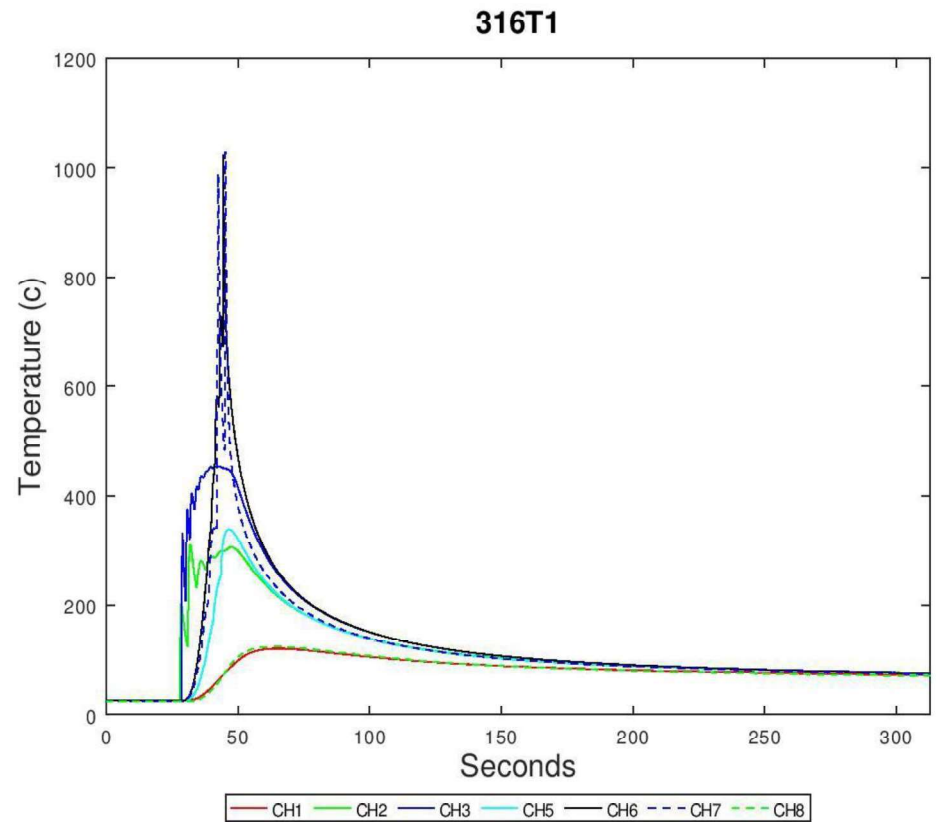
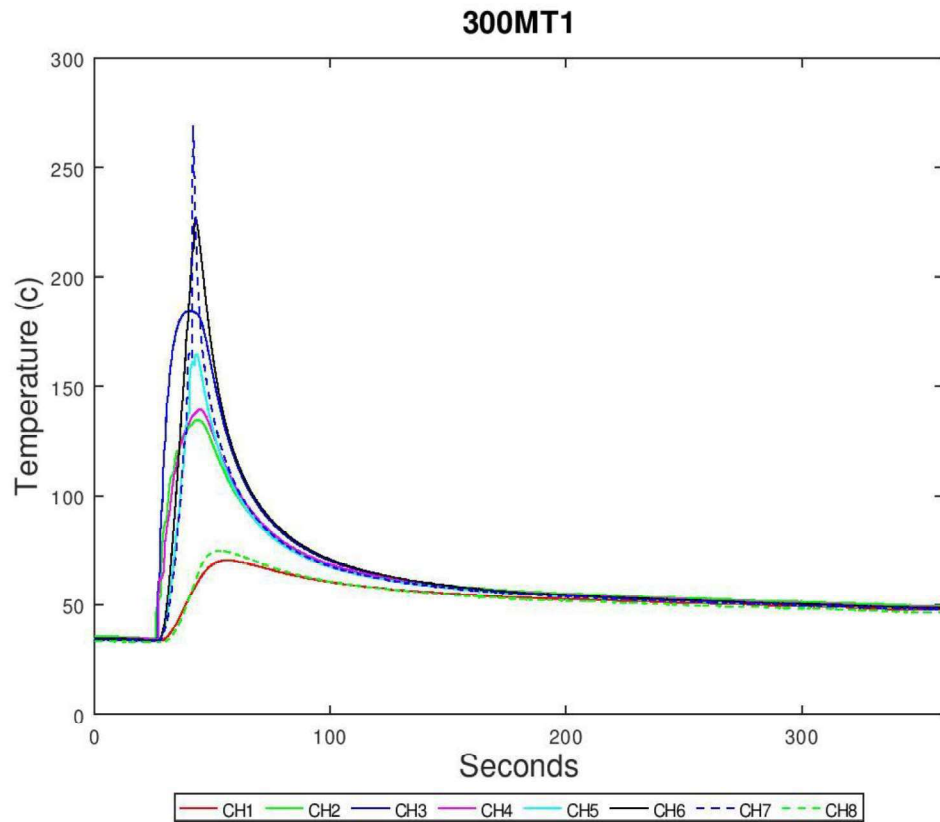
DAQ and Instrumented Sample



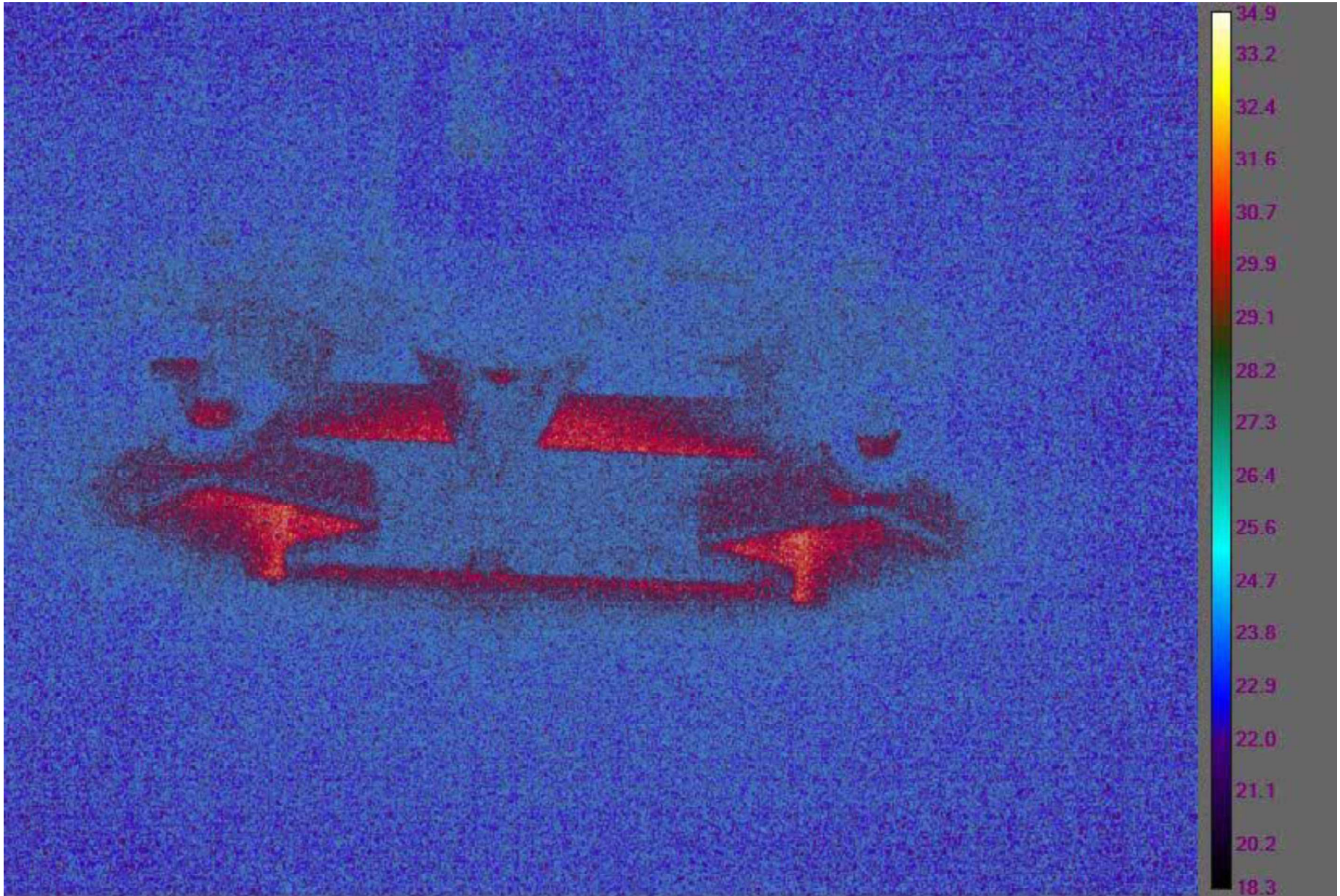
Two Samples after Deposition



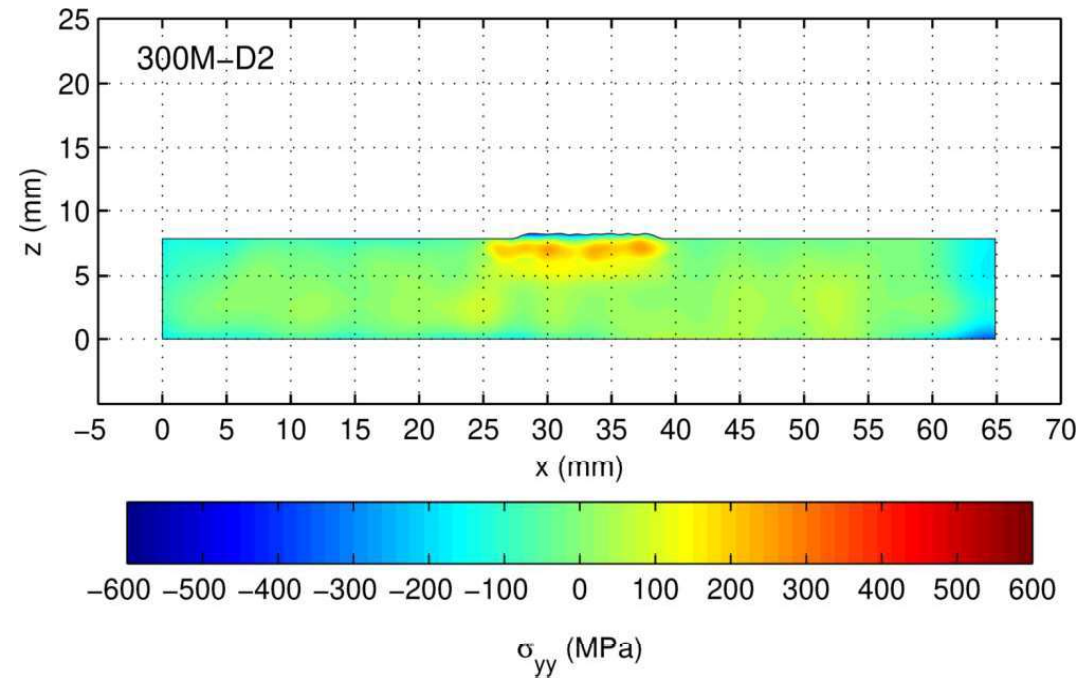
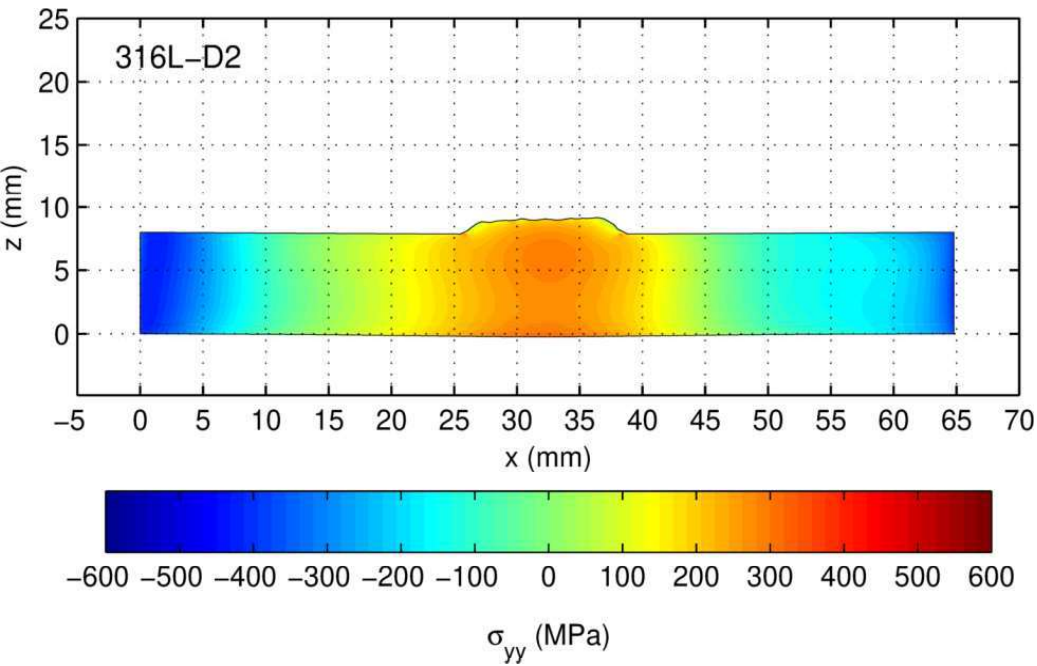
Typical thermocouple data



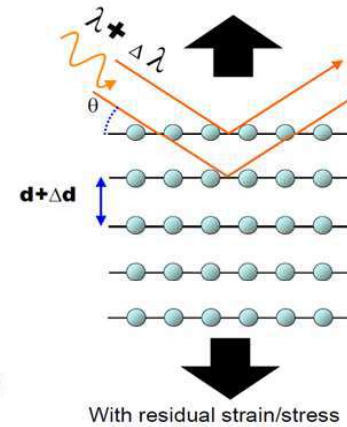
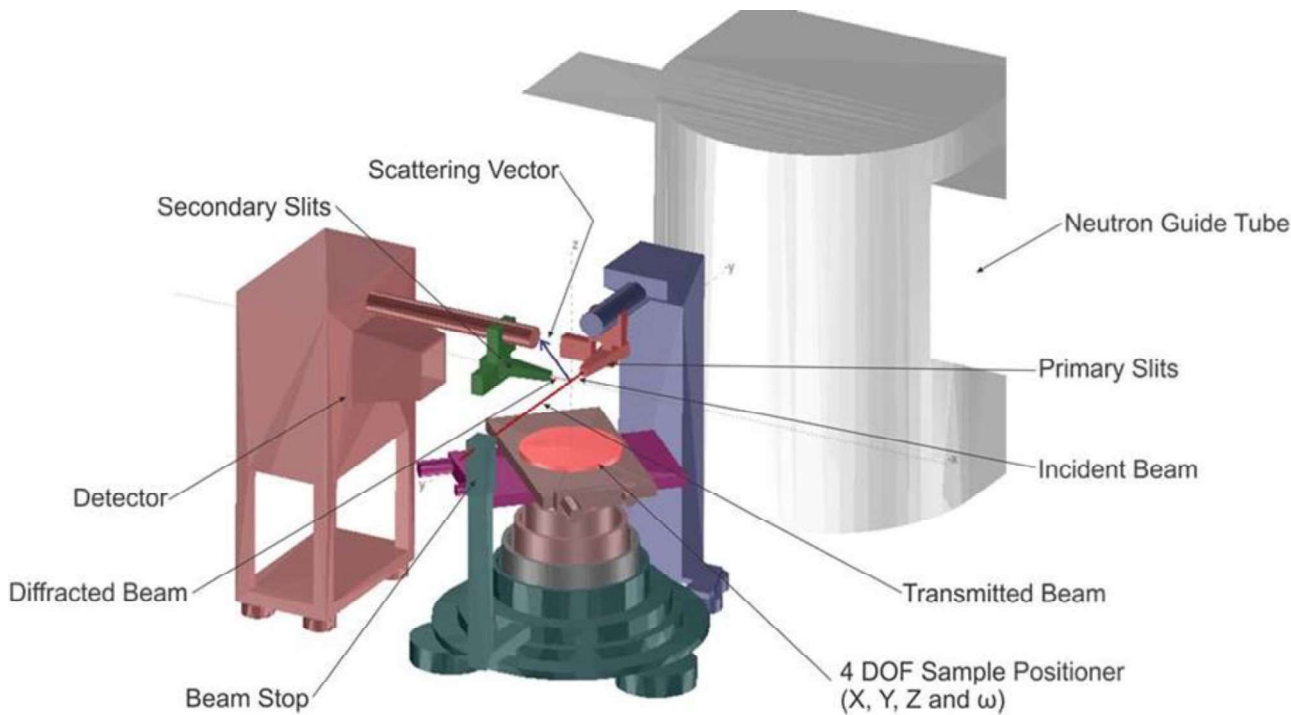
Typical Example Infrared Camera Results



Contour Residual Stress Results

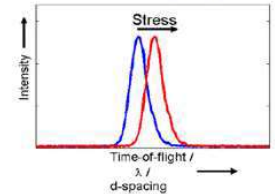


Neutron Diffraction Measurements with Kowari Instrument at ANSTO Lucas heights

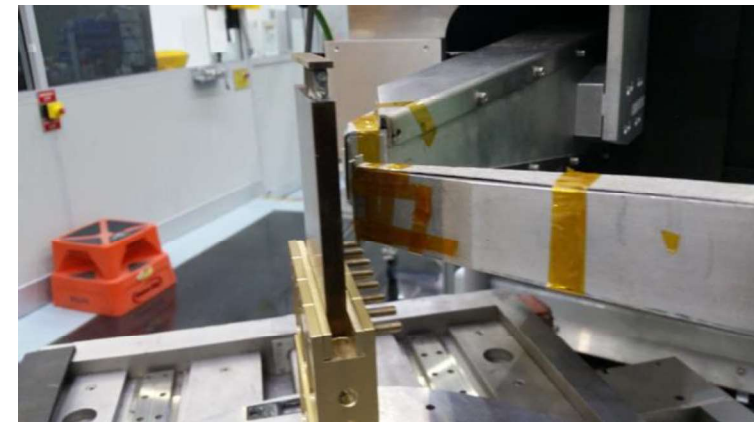


Bragg's Law:
 $d = \lambda / (2 \sin\theta)$

Fixed angle θ : $\epsilon = \frac{\Delta d}{d} = \frac{\Delta \lambda}{\lambda}$

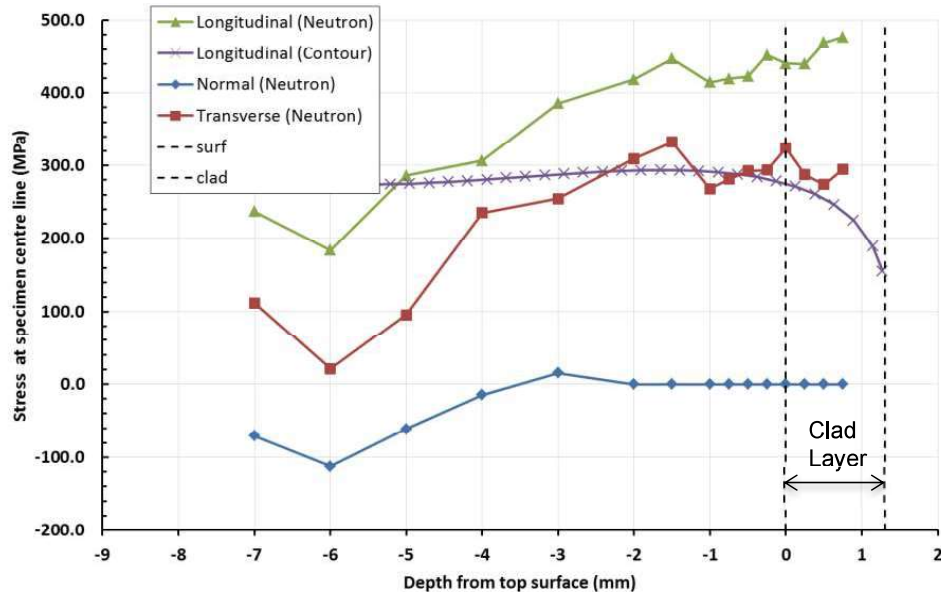


Diffraction peak shift is used to determine residual strain and stress

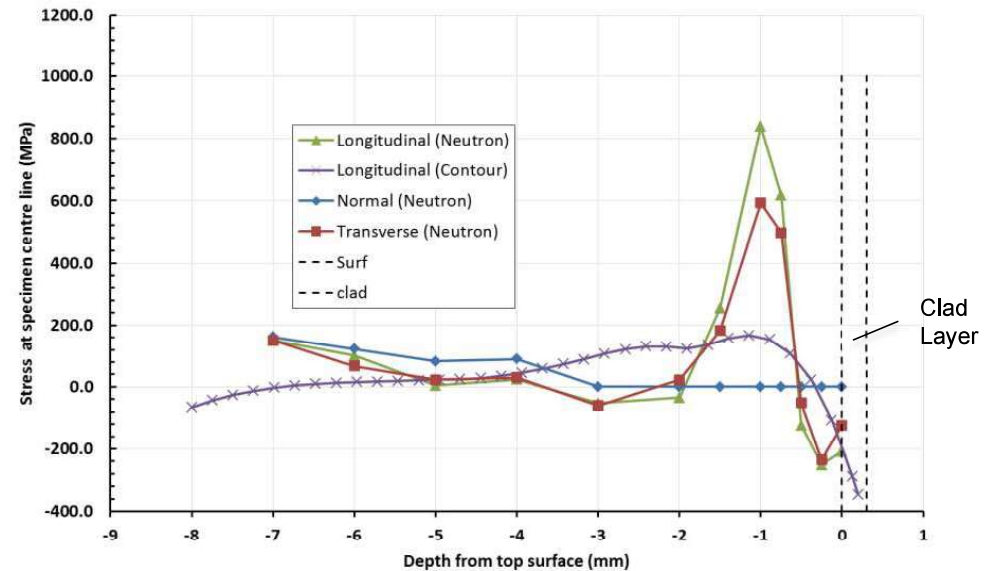


Neutron Diffraction and Contour Measurements

316L Residual Stress Measurements



300M Residual Stress Measurements

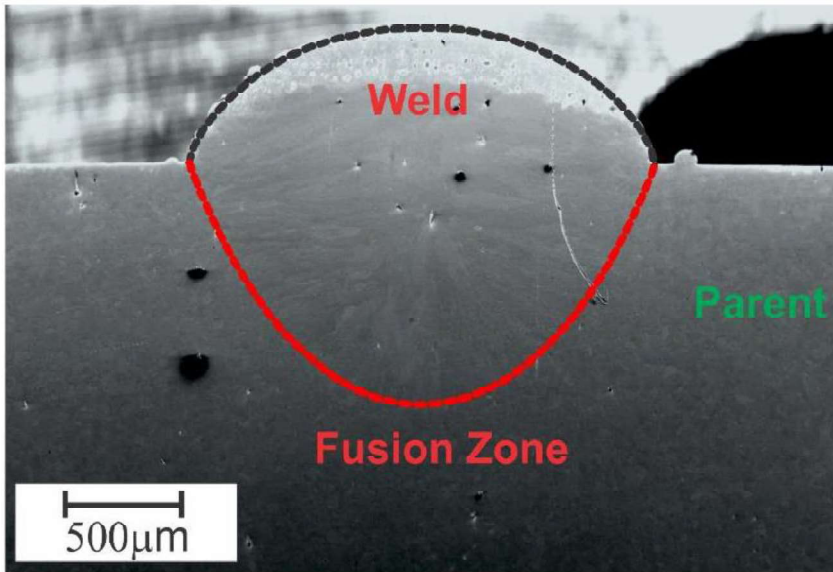


Observations:

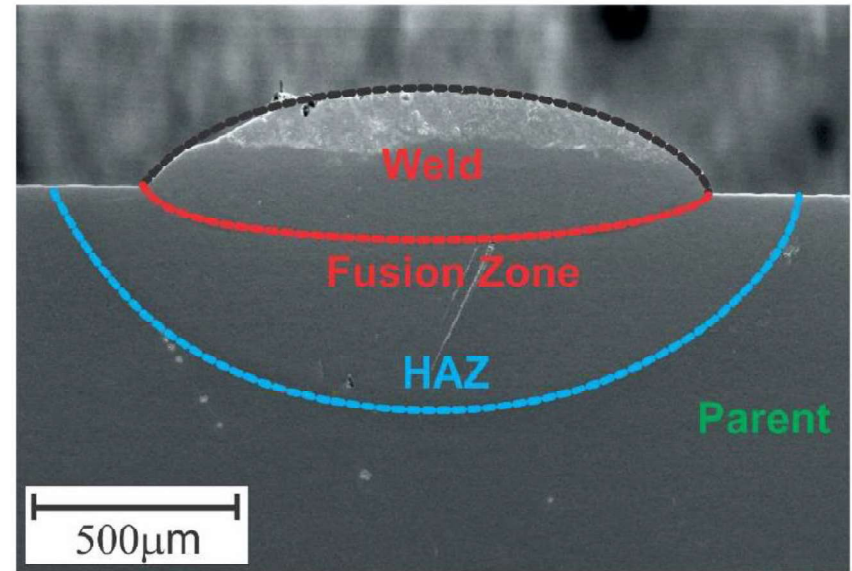
- Contour measurement less reliable near surface
- Both methods detect trend of significant stress gradient from compression to tension in the near-surface for the 300M. Similar to that observed with AerMet®100
- Tension peak for 300M detected with Neutron is localised and may not therefore be detected with the contour method
- Results still being assessed

316L and 300M Fusion Zone

316L Single Pass



300M Single Pass



w/o SSPT

$$\varepsilon_{ij}^t = \varepsilon_{ij}^e + \varepsilon_{ij}^p + \varepsilon_{ij}^{th} + \varepsilon_{ij}^{tr} + \varepsilon_{ij}^{tp}$$

elastic strain

plastic strain

thermal strain

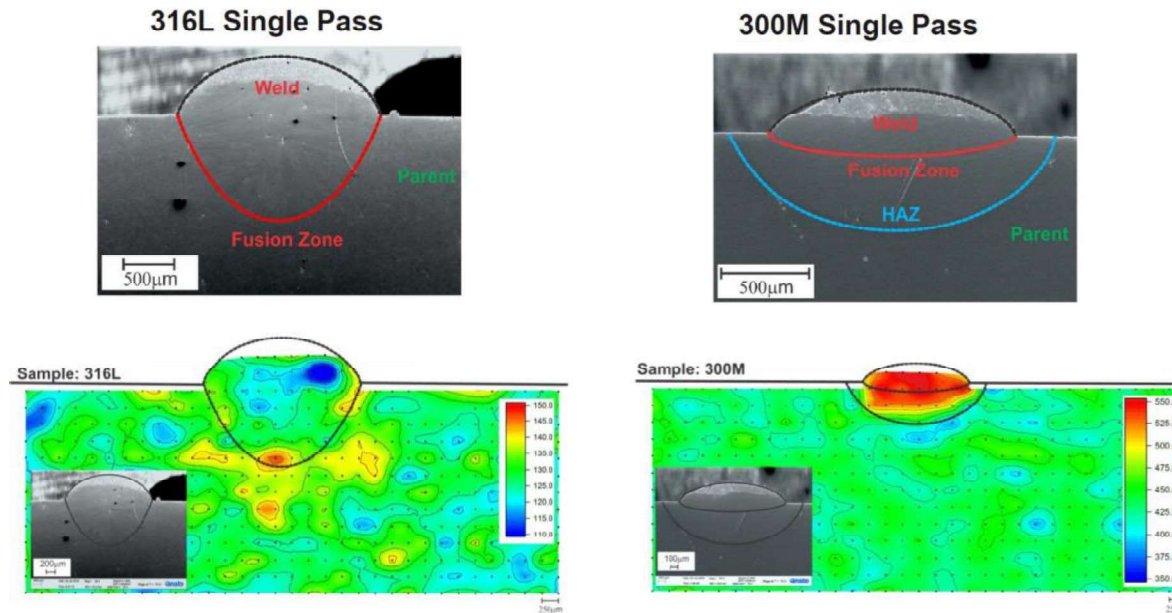
w/ SSPT

$$\varepsilon_{ij}^t = \varepsilon_{ij}^e + \varepsilon_{ij}^p + \varepsilon_{ij}^{th} + \varepsilon_{ij}^{tr} + \varepsilon_{ij}^{tp}$$

metallurgical transformation strain

transformation-induced plastic strain

316L and 300M Hardness

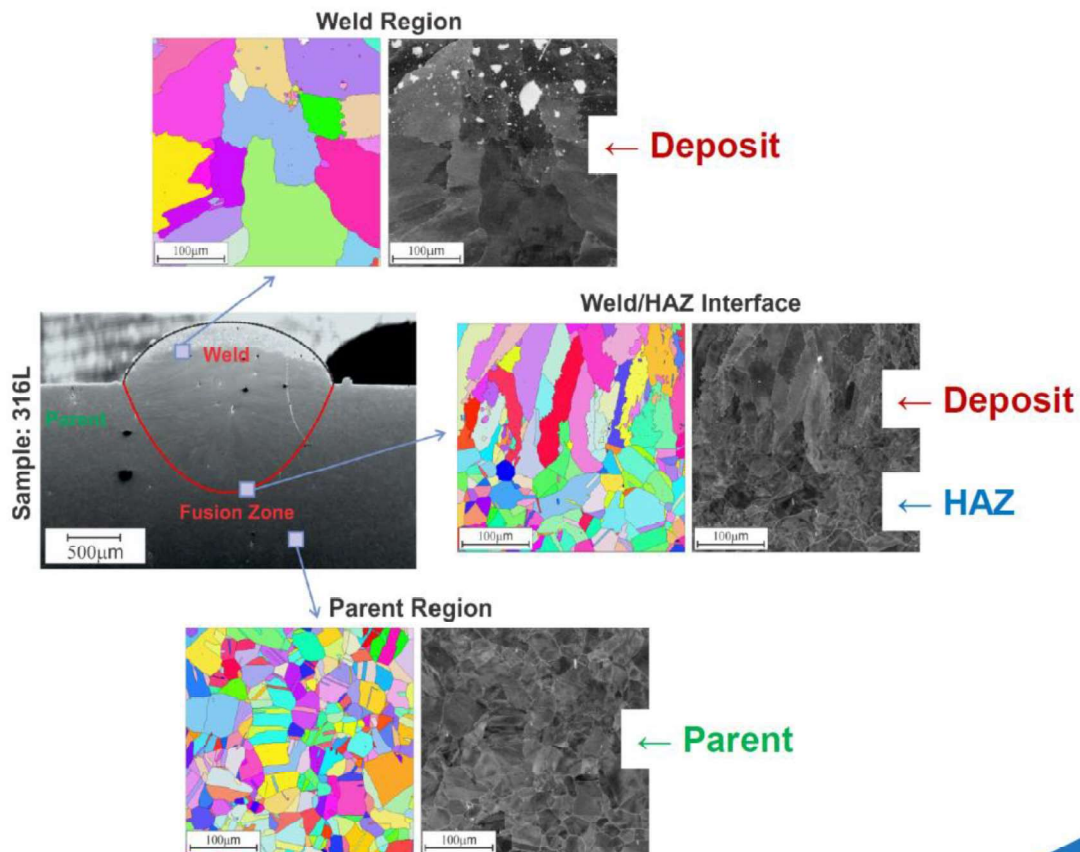


Observations:

- Hardness measured with nano-indenter
- Increased hardness in 300M clad due to fast cooling rate which affects phase transformation and final hardness of martensite
- 316L – no phase transformation and therefore hardness is similar across all regions



316L Cladding Microstructure

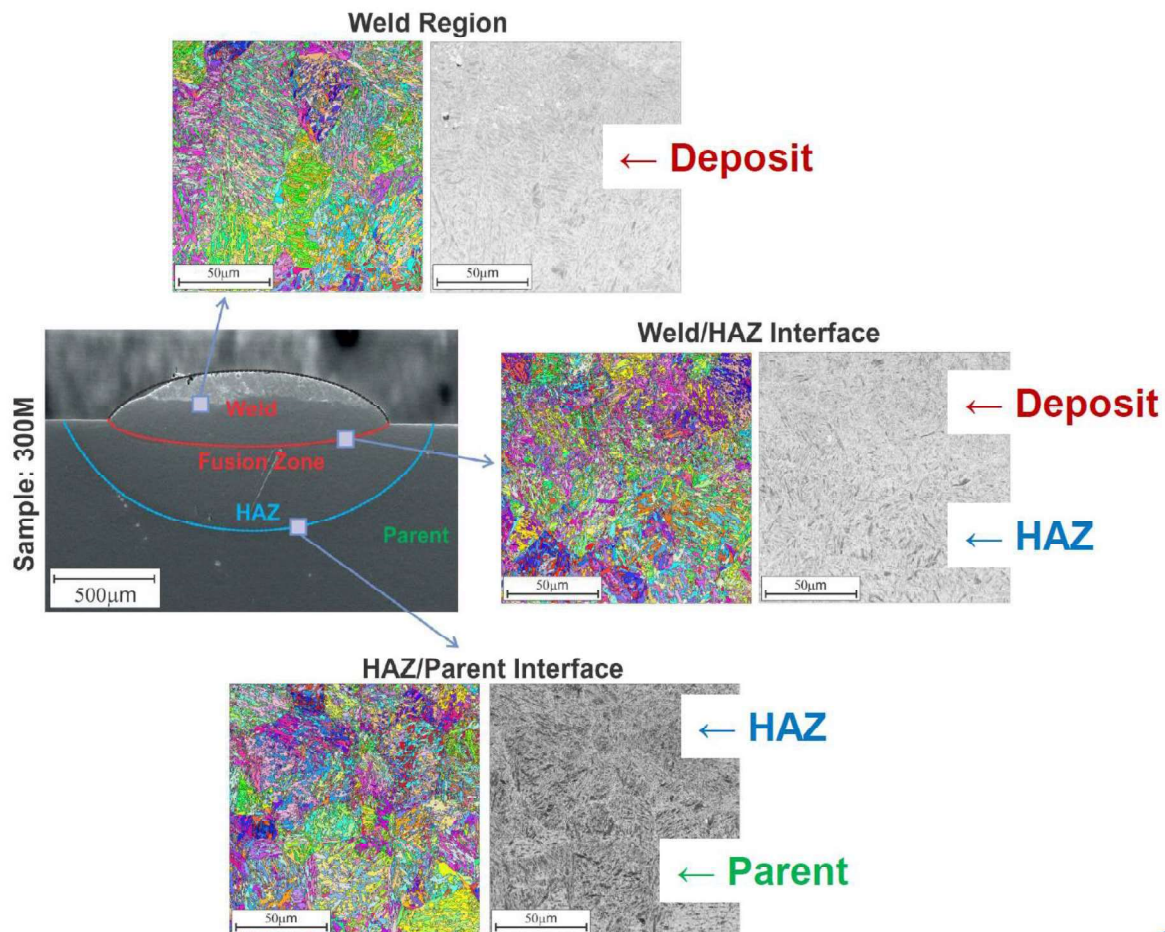


Observations:

- Significantly larger austenite grains in the clad (weld) material compared with the parent
- Austenite grain growth in the direction of heat flow in the weld/HAZ interface region



300M Cladding Microstructure



Observations:

- Microstructure morphology is similar in clad (weld), HAZ and parent
- However, there is evidence of larger prior-austenite grains in the clad (weld) than HAZ and parent material

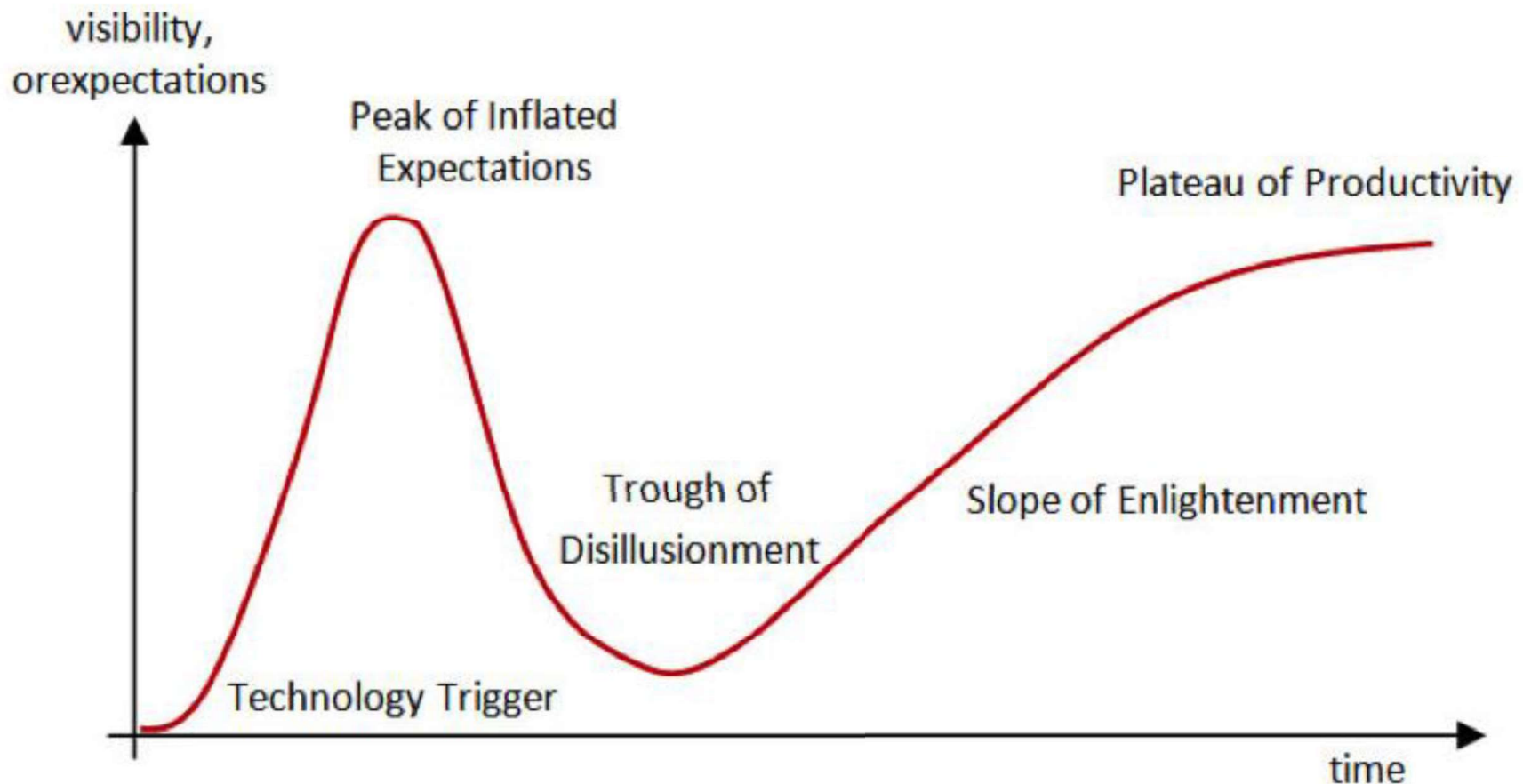


Conclusion and Future Work

- Laser Cladding (LC) is emerging as a viable and attractive structural repair option for critical and expensive steel aerospace components and structures
- Development and validation of modelling to support repair design, substantiation and certification progressing well
- Ongoing and future work includes:
 - Completion of model development for 300M steel
 - Develop the application for an in-service component with representative damage (eg. F-35A nose landing gear piston)
 - Extension to other material systems including Titanium and Aluminium alloys

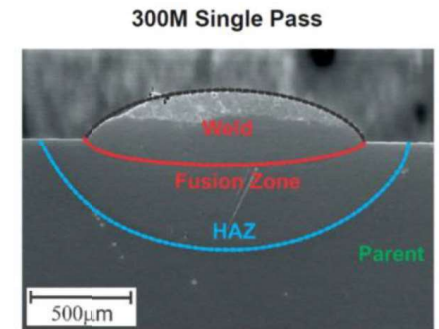
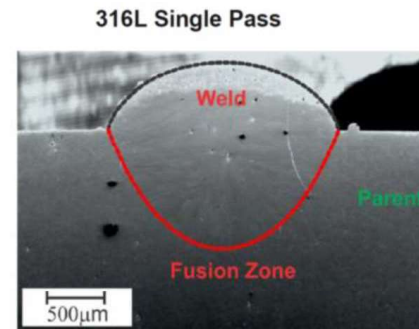
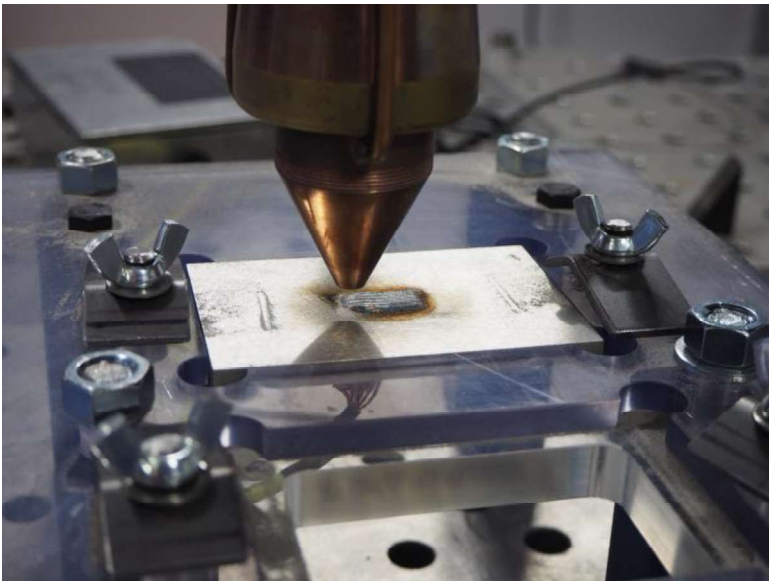
A Challenge for Laser Cladding Repair Application:

- Avoid the “trough of disillusionment” where ongoing investment is needed to mature the technology





Questions?



w/o SSPT

$$\varepsilon_{ij}^t = \varepsilon_{ij}^e + \varepsilon_{ij}^p + \varepsilon_{ij}^{th} + \varepsilon_{ij}^{tr} + \varepsilon_{ij}^{tp}$$

elastic strain plastic strain thermal strain

w/ SSPT

$$\varepsilon_{ij}^t = \varepsilon_{ij}^e + \varepsilon_{ij}^p + \varepsilon_{ij}^{th} + \varepsilon_{ij}^{tr} + \varepsilon_{ij}^{tp}$$

metallurgical transformation strain transformation-induced plastic strain